DEPARTMENT OF THE INTERIOR
UNITED STATES GEOLOGICAL SURVEY

SEISMICITY OF THE SAN FRANCISCO BAY BLOCK, CALIFORNIA

by

Jean A. Olson and Mary Lou Zoback

OPEN-FILE REPORT 95-38

Menlo Park, California
1995

Table of Contents

List of Tables

List of Figures

List of Figures, continued

Introduction

The San Francisco Bay block is bounded by two major 30°-35°NW-trending right-lateral strike-slip fault systems, the San Andreas and Hayward faults, which accommodate most of the relative motion between the Pacific and North American plates at this latitude (37.4°N-38°N) (Figure 1a). Present-day seismicity (during the past 26 years) in the San Francisco Bay area is generally associated with the San Andreas and Hayward-Calaveras fault systems, but a persistent, albeit low level, of microseismicity has also occurred within the 30-km-wide block bounded by these fault zones (Figure 1b). San Francisco Bay occupies a relative structural depression within this block (Page, 1982).

Geodetic and geologic evidence suggest that much of the relative Pacific-North American plate motion is accommodated by major (M≥6.8) earthquakes on the San Andreas and Hayward fault systems. Presently, the central portion of the Hayward fault slips aseismically (creeps) at an average rate of about 4-6 mm/yr (over the past two decades) (Lienkaemper et al., 1991) and produces background seismicity (M≤4.5 during the past 26 years) (Oppenheimer et al., 1992). The segment of the San Andreas fault between the Golden Gate Bridge and the Loma Prieta aftershock zone (see Figure 1b), however, is essentially locked -- this segment has produced only a low-level of background seismicity (M≤4.4) along the 45-km-long portion north of Crystal Springs Reservoir (Olson and Zoback, 1992). In the southern part of the San Francisco peninsula and the East Bay, off-fault background seismicity appears to accommodate a small component of NE-SW convergence (Olson and Zoback, 1992; Oppenheimer and MacGregor-Scott, 1992; Kovach and Beroza, 1993).

In contrast, evidence is ambiguous for Holocene deformation within the Bay block proper, and the cause of broader-scale deformation related to the formation of the San Francisco Bay basin within the Bay block has not been identified. Geodetic observations in the past two decades limit shear strain rates within the block to <3 mm/yr, which is within the noise level for those observations (Lisowski et al., 1991). Thus, if any active faults exist within the Bay block, they must have long (thousands of years) recurrence intervals. Geologic mapping provides equivocal evidence for Holocene faulting within the onshore portion of the block except for small thrust faults subparallel to and within 5 km of the major strike-slip faults (Hart et al., 1981; Page, 1992).

Large-scale, through-going fault zones within the Bay block were suggested by Brabb and Hanna (1981) on the basis of prominent linear N50°-60°W-trending aeromagnetic anomalies (Figure 2) aligned with mapped onshore shear zones within the Franciscan Formation (Figure 1a). Both gravity data (Figure 3) and recent high-resolution seismic-reflection profiles of Holocene Bay mud rule out significant vertical offsets across these proposed fault zones, however, and the seismic-reflection data also appear to rule out any significant Holocene strike-slip offset along these fault zones (Marlow et al., 1995). Preliminary interpretation of high-resolution seismic-reflection profiles in the San Francisco Bay had indicated two broad, NW-trending Holocene fault zones within the upper 10-50 m of Bay mud (Mann et al., 1993), which generally coincided with the linear aeromagnetic anomalies. However, evidence for the two postulated fault zones were subsequently revealed to be caused by lateral changes in amplitude brightness (possibly due to biogenic gas) coupled with a long source duration (Marlow et al., 1995). Even though the seismic-reflection evidence for "mud faults" has disappeared, the possibility of through-going faults or shear zones in the Franciscan basement beneath the bay mud suggested by Brabb and Hanna (1981) remains. However, the lack of observable shear strain within the Bay block and the lack of Holocene offset across these postulated fault zones suggests that, if these magnetic anomalies are indeed associated with pre-existing basement faults, they are probably relict structures which are currently inactive.

Despite the present low seismicity levels within the Bay block and the equivocal evidence for slip on the proposed intrablock fault zones, the proximity of the Bay block to major metropolitan centers and critical lifelines requires that the potential hazard due to any future earthquakes within the block be assessed, as even a moderate earthquake in this area could pose a significant hazard. Seismicity is one independent means by which active faulting can be identified and, in this study, we examine the spatio-temporal patterns and source character of this microseismicity and investigate its possible association with the proposed intrablock fault zones on the basis of any correlative hypocentral locations and fault-plane solutions. Results of

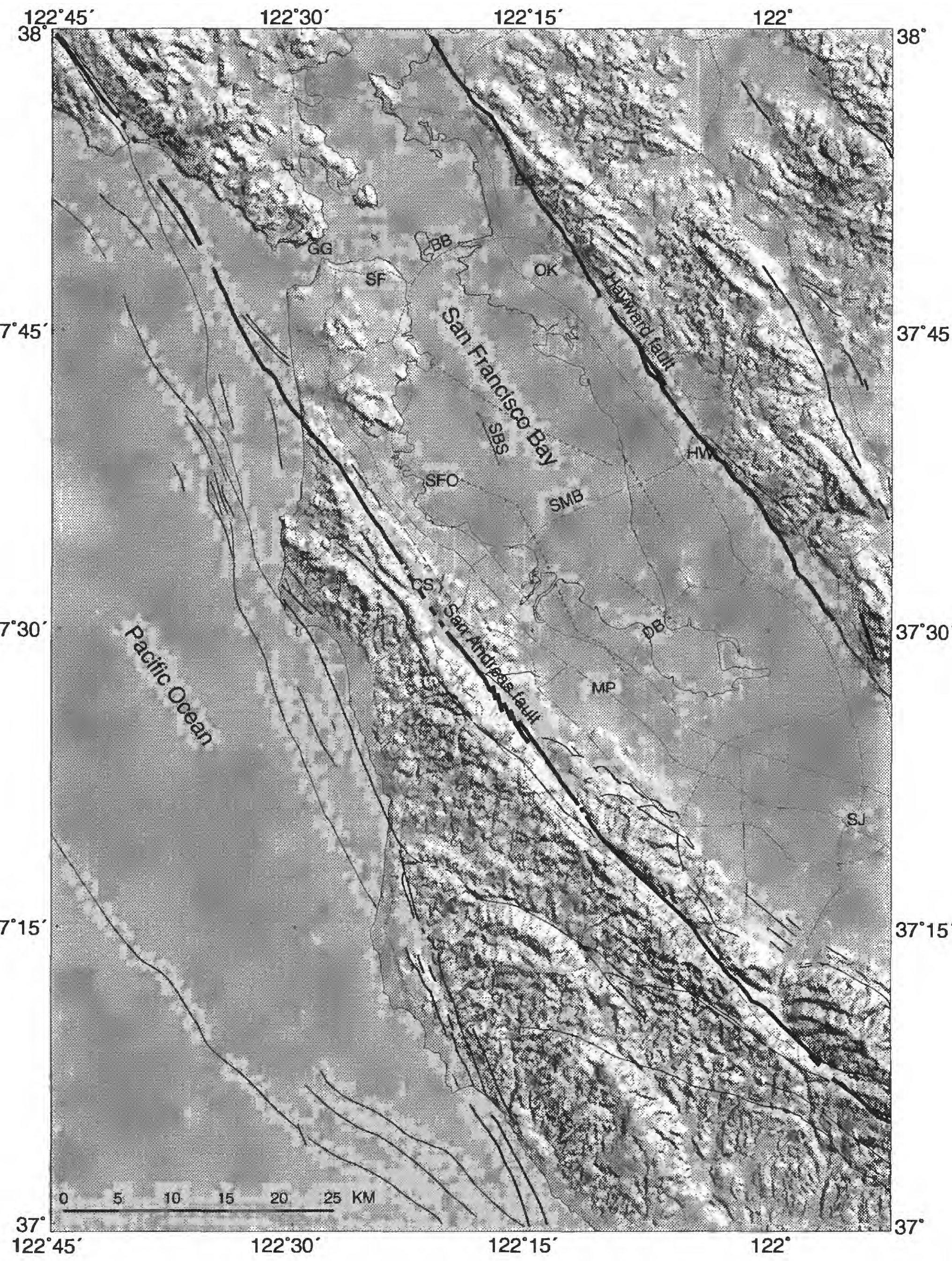

Figure 1a. Map of San Francisco Bay area Quaternary faults. Heavy line in bay shows axis of San Bruno shoal (SBS), an anticlinal-shaped bathymetric high on the bay floor, possibly tectonic or a remanent levee; dashed lines in bay show axes of aeromagnetic anomaly highs; thin lines show major roads and freeways. BB, Bay Bridge; BK, Berkeley; CS, Crystal Springs Reservoir; DB, Dumbarton Bridge; GG, Golden Gate Bridge; HW, Hayward; MP, Menlo Park; OK, Oakland; SF, San Francisco; SFO, San Francisco airport; SMB, San Mateo Bridge.

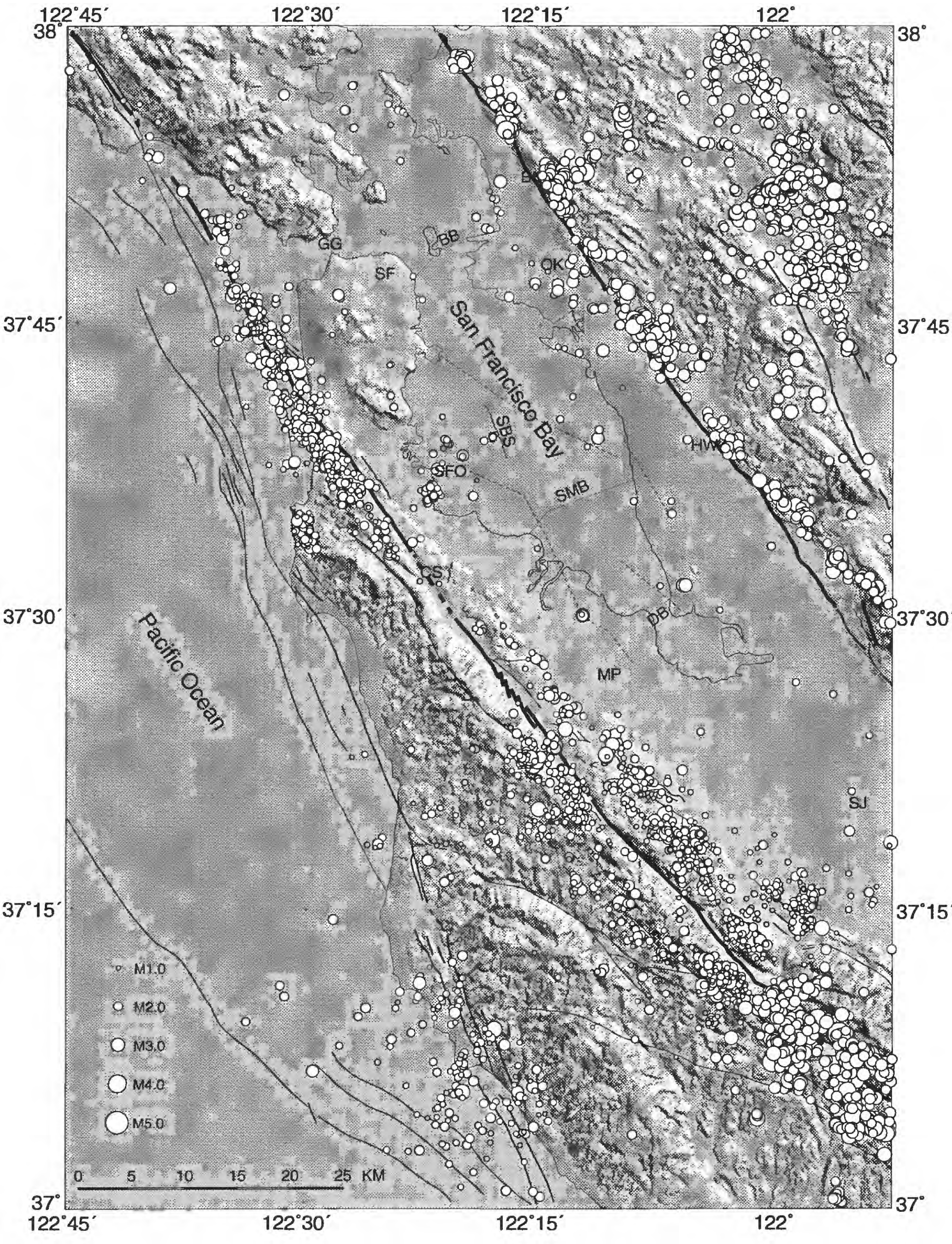

Figure 1b. Map showing relocated M≥1 epicenters (open circles) in the San Francisco peninsula (Olson and Zoback, 1992) and San Francisco Bay block areas (this study), and NCSN catalog M≥2 epicenters in the East Bay area during the past 26 years (January 1, 1969 through November 25, 1994). Epicenter circles are scaled linearly, proportional to magnitude. All events located with at least 6 arrival times and have RMS travel-time residual ≤0.3 s, estimated horizontal error (ERH) ≤2 km, estimated vertical error ≤4 km and minimum station distance <20 km. Heavy line in bay shows axis of San Bruno shoal (SBS); dashed lines in bay show axes of aeromagnetic anomaly highs; thin lines in bay show bridges. Concentration of epicenters along the San Andreas fault zone SE of 37°10' is northern end of Loma Prieta aftershock zone.

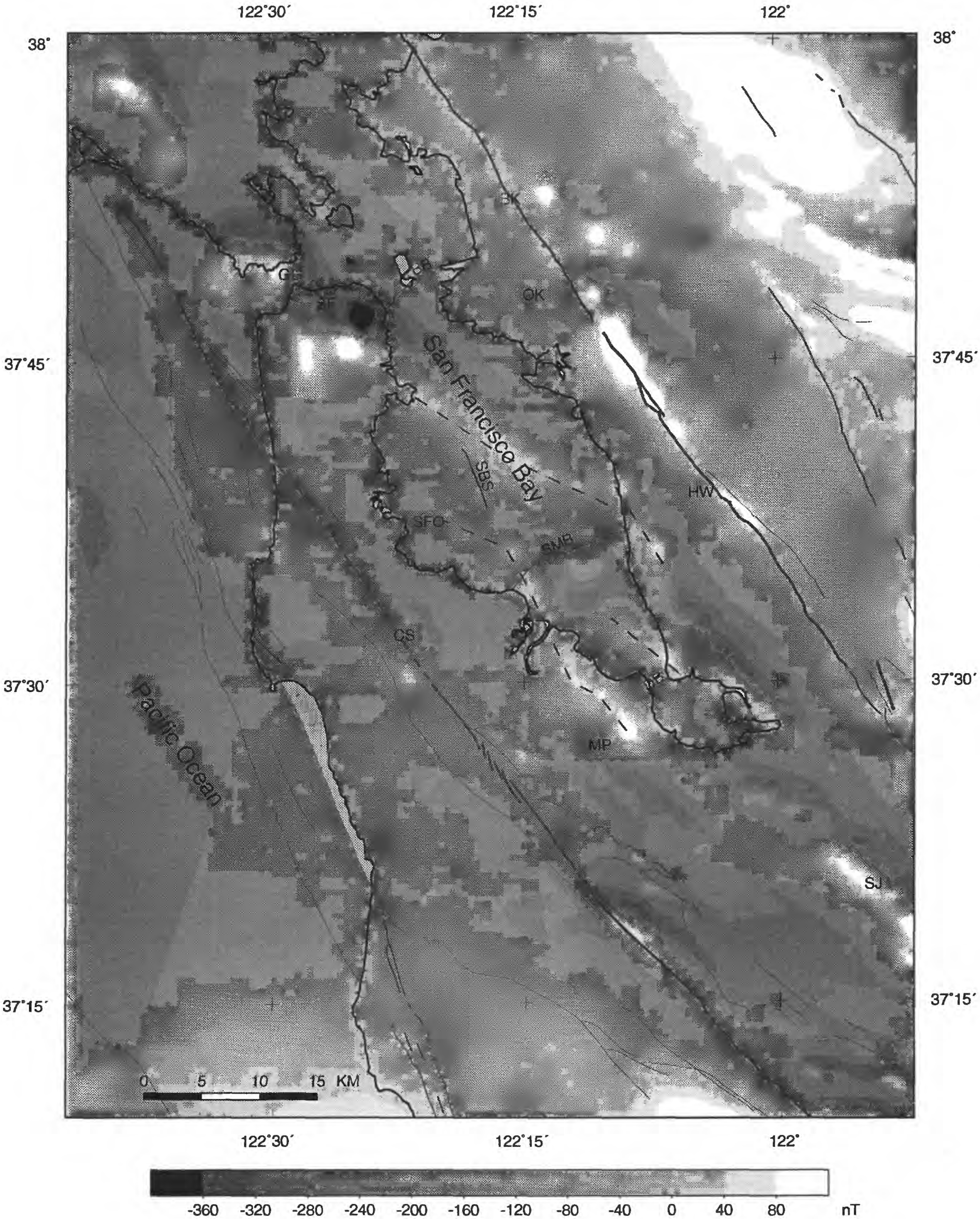

Figure 2. Aeromagnetic map of the San Francisco Bay area; data from Jachens and Roberts (1993). Heavy line in bay shows axis of San Bruno shoal (SBS); dashed lines in bay show axes of aeromagnetic anomaly highs; thin lines in bay show bridges.

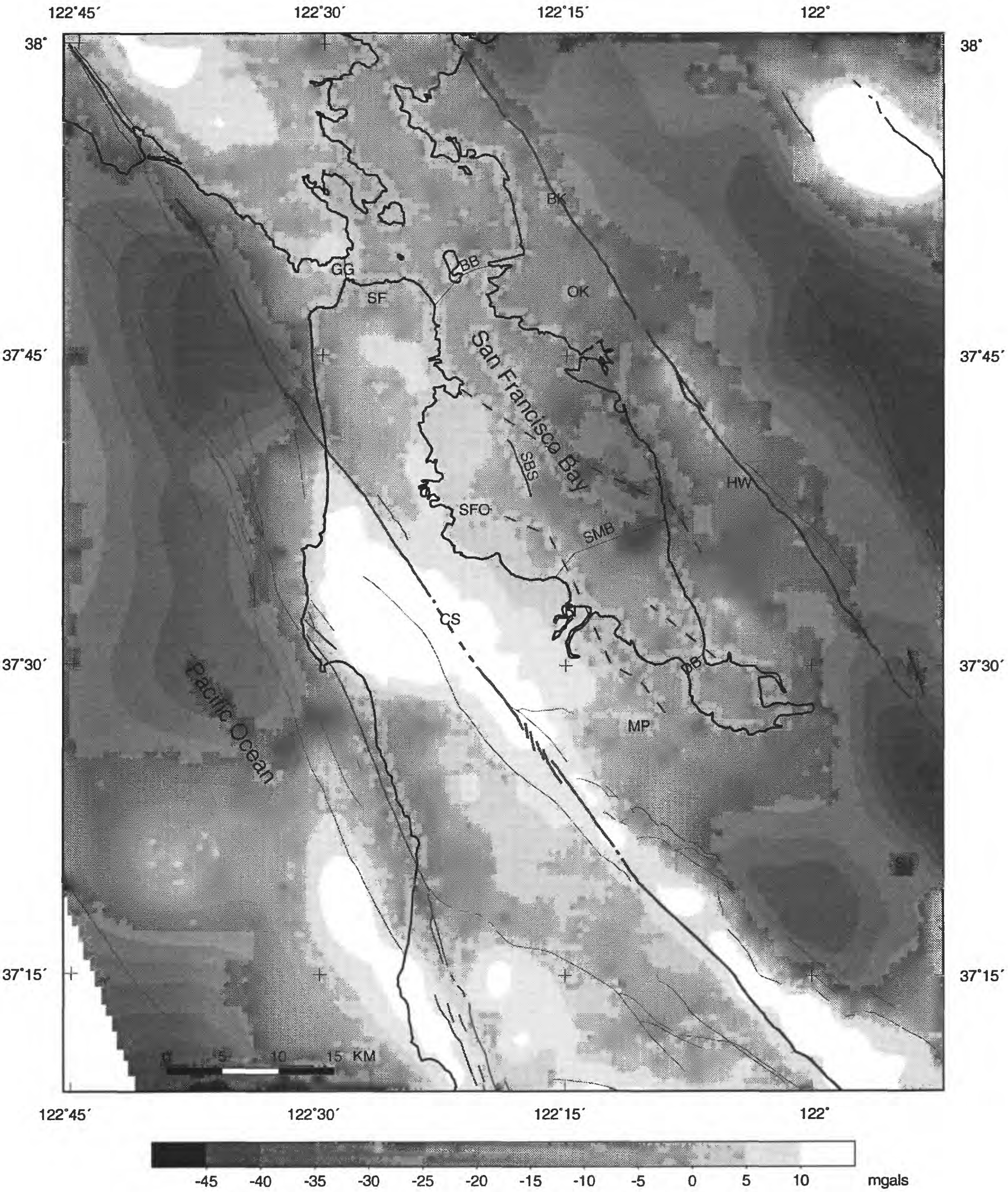

Figure 3. Isostatic residual gravity map of the San Francisco Bay area; data from Roberts and Jachens (1993). Heavy line in bay shows axis of San Bruno shoal (SBS); dashed lines in bay show axes of aeromagnetic anomaly highs; thin lines in bay show bridges.

this study are, however, largely negative as we find no obvious correlation of seismicity with the proposed transbay fault zones. Furthermore, the seismicity does not suggest any other possible large-scale fault zones within the Bay block. Despite these negative results, this study forms a small but important step toward assessing the potential earthquake hazard in the Bay block.

Data Analysis and Relocation Procedure

Data collection and location analysis

We selected a study area between the San Andreas and Hayward fault surface traces at the latitudes of the the San Francisco Bay, between 37.42°N-38°N latitude. Standard processing of the USGS Northern California Seismic Network (NCSN) (e.g. Oppenheimer et al., 1993) had located 178 earthquake hypocenters within the study area between January 1, 1969 and November 25, 1994 using a series of one-dimensional (1-D) regional velocity models and station corrections based on earthquake travel-times. Separate 1-D velocity models are used for the San Francisco peninsula and for the Hayward fault, and a smoothed average of those two models is used to locate events in the intermediate area beneath San Franciscco Bay. However, since these models were calculated, additional independent velocity information became available for the immediate San Francisco Bay region from a marine seismic-reflection/refraction profile collected along the axis of the Bay as part of the 1991 Bay Area Seismic Experiment (BASIX) (McCarthy and Hart, 1993), as well as from other controlled-source travel-time data collected during two active, onshore seismic-reflection and refraction experiments in 1991 and 1993 (Murphy et al., 1992; Kohler and Catchings, 1994).

We used this new velocity information to attempt to improve hypocentral locations in the study area. First, we used a 1-D velocity model (Figure 4) based on the 2-D velocity model of Hole et al. (1993) for the San Francisco Bay seismic-refraction/reflection profile, and station corrections within the Bay block that we calculated specifically for this model. These station corrections are time adjustments for each station, applied to earthquake travel-times, which correct for differences between the model and true velocities in the upper ~15 km of the crust averaged along the sampled raypaths to each station, and are typically in the range +/-0.5 s for an area the size of the Bay block.

We calculated station corrections for this (fixed) 1-D model using VELEST, a least-squares, joint hypocenter-velocity travel-time inversion procedure (Ellsworth, 1977; Roecker, 1981). Station corrections were calculated for a total of 57 stations (see Table 1) and 44 sources (Table 2) within the Bay block (Figure 5), with epicentral distances within 50 km. These station corrections are relative to a fixed station correction (0 s) for the two stations located near the eastern end of the Dumbarton Bridge "CCYM" and "CYHM" (see Figure 5 and Table 1). A total of 562 P-wave travel-time observations from 21 earthquakes, 16 quarry blasts and 7 USGS onshore seismic experiment shots were used in the inversion. The shot locations and origin times were held fixed and the earthquake and quarry blast locations and origin times were solved for.

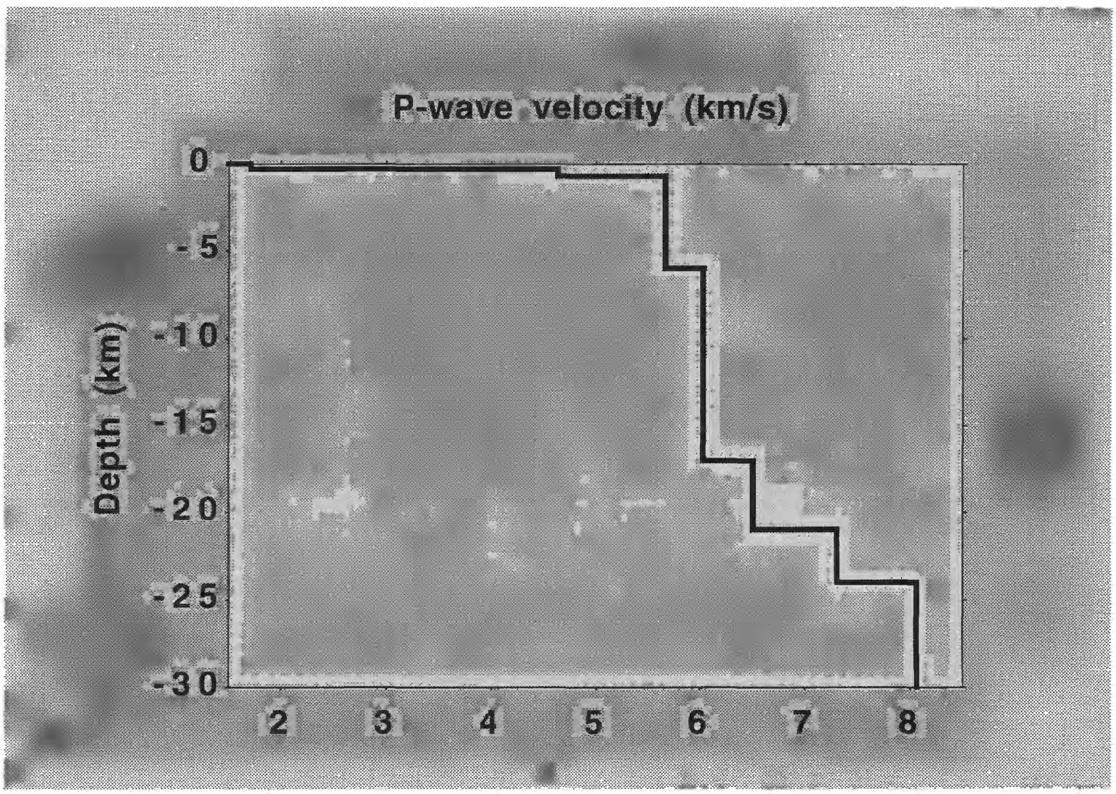

Figure 4. One-dimensional P-wave velocity model for crust in San Francisco Bay block (Steven Holbrook, written communication, 1994), based on two-dimensional velocity model calculated for NW-trending San Francisco Bay seismic-reflection/refraction profile (Hole et al., 1993).

Table 1. USGS Northern California Seismic Network (NCSN) Stations used to locate earthquakes in this study (C, component; SC, station correction in seconds).

CODE	LATIDUTE	LONGITUDE	C	SC	POLARITY REVERSAL PERIOD*
BKSB	37N°52.60'	122W°14.10'	Z	0.35	
BKSB	37N°52.60'	122W°14.10'	E	0.35	
BKSB	37N°52.60'	122W°14.10'	N	0.35	
BRKB	37N°52.40'	122W°15.60'	Z	0.35	
CAIM	37N°51.68'	122W°25.77'	Z	0.23	
CALM	37N°27.07'	121W°47.95'	Z	0.07	720607-740405
CALM	37N°27.07'	121W°47.95'	E	0.07	
CALM	37N°27.07'	121W°47.95'	N	0.07	
CBKM	37N°52.56'	122W°14.88'	Z	0.35	
CBRM	37N°48.97'	122W° 3.72'	Z	0.50	750715-751107
CBRM	37N°48.97'	122W° 3.72'	N	0.50	
CBWM	37N°55.45'	122W° 6.40'	Z	0.80	
CCNM	37N°47.49'	121W°56.89'	Z	0.96	
CCOM	37N°15.46'	121W°40.35'	Z	0.28	740717-830727
CCRM	37N°47.30'	121W°57.00'	Z	0.96	700923-720609
CCYM	37N°33.10'	122W° 5.45'	Z	0.00	
CDAL	37N°43.80'	121W°43.70'	Z	0.84	
CDAL	37N°43.80'	121W°43.70'	E	0.84	
CDOM	37N°43.80'	121W°50.12'	Z	1.09	
CDSM	37N°57.98'	122W°15.17'	Z	0.49	
CDUM	38N° 1.78'	122W° 0.05'	Z	1.35	
CDUM	38N° 1.78'	122W° 0.05'	N	1.35	
CDVL	37N°33.98'	121W°40.81'	E	0.31	
CDVL	37N°33.98'	121W°40.81'	N	0.31	
CDVL	37N°33.98'	121W°40.81'	N	0.31	
CDVL	37N°33.98'	121W°40.81'	E	0.31	
CDVL	37N°33.98'	121W°40.81'	Z	0.31	
CDVL	37N°33.98'	121W°40.81'	Z	0.31	
CGPM	37N°38.72'	122W° 0.62'	Z	0.17	
CGPM	37N°38.72'	122W° 0.62'	Z	0.17	
CLCM	37N°44.28'	122W° 3.83'	Z	0.38	
CMCM	37N°46.88'	122W°10.55'	Z	0.20	
CMHM	37N°21.57'	121W°45.38'	Z	0.11	
CMJM	37N°31.25'	121W°52.23'	Z	0.15	
CMKM	37N°29.13'	121W°51.93'	N	0.15	
CMKM	37N°29.13'	121W°51.93'	E	0.15	
CMKM	37N°29.13'	121W°51.93'	Z	0.15	
CMLM	37N°28.64'	121W°39.09'	Z	0.15	
CMNL	37N°37.65'	121W°42.50'	Z	0.85	
CMNL	37N°37.65'	121W°42.50'	E	0.85	
CMNL	37N°37.65'	121W°42.50'	N	0.85	
CMOM	37N°48.68'	121W°48.15'	Z	1.04	
CMRM	37N°35.68'	121W°38.22'	Z	0.30	
CNIM	37N°36.47'	121W°57.84'	E	0.22	
CNIM	37N°36.47'	121W°57.84'	Z	0.22	
CPAM	37N°37.88'	121W°57.37'	Z	0.22	
CPIM	37N°59.33'	122W°12.88'	Z	0.86	
CPLM	37N°38.25'	121W°57.64'	Z	0.22	
CPMM	37N°56.94'	122W°24.46'	Z	0.20	
CRAM	37N°46.03'	121W°56.25'	Z	1.02	

Table 1, continued. USGS Northern California Seismic Network (NCSN) Stations used to locate earthquakes in this study (C, component; SC, station correction in seconds).

CODE	LATIDUTE	LONGITUDE	C	SC	POLARITY REVERSAL PERIOD*
CRPM	37N°54.75'	121W°54.33'	Z	0.63	
CSAL	37N°40.42'	121W°42.25'	E	0.92	
CSAL	37N°40.42'	121W°42.25'	N	0.92	
CSAL	37N°40.42'	121W°42.25'	Z	0.92	
CSCM	37N°17.11'	121W°46.35'	Z	0.24	730904-831003
CSHM	37N°38.88'	122W° 2.57'	Z	0.17	740712-740806
CSLM	37N°43.46'	122W° 7.10'	E	0.38	
CSLM	37N°43.46'	122W° 7.10'	N	0.38	
CSLM	37N°43.46'	122W° 7.10'	Z	0.38	
CSPM	37N°57.45'	122W°18.65'	Z	0.49	
CSVM	37N°51.88'	122W° 0.16'	Z	1.20	
CVAL	37N°37.10'	121W°45.49'	N	0.55	
CVAL	37N°37.10'	121W°45.49'	Z	0.55	
CVLL	37N°37.58'	121W°50.14'	E	0.72	690101-881204*
CVLL	37N°37.58'	121W°50.14'	Z	0.72	
CVLL	37N°37.58'	121W°50.14'	N	0.72	
CVPM	37N°53.04'	122W°13.32'	Z	0.35	
CVPM	37N°53.04'	122W°13.32'	N	0.35	
CVPM	37N°53.04'	122W°13.32'	E	0.35	
CYBM	37N°48.48'	122W°21.65'	Z	0.16	
CYBM	37N°48.48'	122W°21.65'	E	0.16	
CYBM	37N°48.48'	122W°21.65'	N	0.16	
CYBM	37N°48.48'	122W°21.65'	Z	0.16	
CYHM	37N°33.54'	122W° 5.62'	Z	0.00	
HVSG	37N°20.28'	121W°42.84'	Z	0.11	
JALM	37N° 9.50'	121W°50.82'	E	-0.16	
JALM	37N° 9.50'	121W°50.82'	Z	-0.16	700923-911031
JALM	37N° 9.50'	121W°50.82'	Z	-0.16	
JALM	37N° 9.50'	121W°50.82'	N	-0.16	
JBCM	37N° 9.62'	122W° 1.57'	Z	0.13	760325-830523
JBEM	37N°20.54'	122W°20.31'	Z	0.49	
JBGM	37N°20.52'	122W°20.34'	Z	0.49	760924-770128, 901016-910924
JBKM	37N°18.95'	122W° 9.83'	Z	0.08	
JBLM	37N° 7.69'	122W°10.08'	Z	-0.04	
JBLM	37N° 7.69'	122W°10.08'	E	-0.04	
JBLM	37N° 7.69'	122W°10.08'	Z	-0.04	
JBLM	37N° 7.69'	122W°10.08'	N	-0.04	
JBLM	37N° 7.67'	122W° 9.98'	Z	-0.04	
JBMM	37N°19.09'	122W° 9.16'	Z	0.08	
JCHM	37N°31.02'	122W°22.56'	E	0.12	
JCHM	37N°31.02'	122W°22.56'	Z	0.12	
JCHM	37N°31.02'	122W°22.56'	N	0.12	
JCPM	37N°35.29'	122W°19.33'	Z	0.23	
JHPM	37N°26.65'	122W°18.09'	Z	0.32	801103-820923
JJRM	37N°20.68'	122W°12.09'	Z	0.05	
JLTM	37N°21.22'	122W°12.25'	Z	0.05	
JLXM	37N°12.11'	121W°59.17'	Z	-0.06	
JMGM	37N°38.22'	122W°28.43'	Z	0.16	
JMOM	37N°27.01'	122W°11.00'	Z	0.12	
JMPM	37N°27.33'	122W° 9.93'	E	0.12	

Table 1, continued. USGS Northern California Seismic Network (NCSN) Stations used to locate earthquakes in this study (C, component; SC, station correction in seconds).

CODE	LATIDUTE	LONGITUDE	C	SC	POLARITY REVERSAL PERIOD*
JMPM	37N°27.33'	122W° 9.93'	Z	0.12	
JMPM	37N°27.33'	122W° 9.93'	E	0.12	
JMPM	37N°27.33'	122W° 9.93'	N	0.12	
JMPM	37N°27.33'	122W° 9.93'	N	0.12	
JMPM	37N°27.33'	122W° 9.93'	Z	0.12	
JPPM	37N°15.87'	122W°12.78'	Z	0.39	811124-831118
JPPM	37N°15.81'	122W°12.78'	Z	0.39	
JPRM	37N°47.68'	122W°28.46'	Z	0.36	
JPRM	37N°47.70'	122W°28.43'	Z	0.36	
JPSM	37N°11.94'	122W°20.90'	Z	0.33	
JRIM	37N°47.28'	122W°23.37'	Z	0.16	
JSAM	37N°34.95'	122W°25.03'	Z	0.23	
JSBM	37N°40.74'	122W°23.80'	Z	0.10	
JSCM	37N°17.07'	122W° 7.42'	Z	0.07	710524-710920
JSFM	37N°24.31'	122W°10.55'	E	0.22	
JSFM	37N°24.31'	122W°10.55'	Z	0.22	700923-720418, 850320-850517
JSFM	37N°24.31'	122W°10.55'	Z	0.22	
JSFM	37N°24.31'	122W°10.55'	N	0.22	
JSGM	37N°16.96'	122W° 3.00'	Z	0.50	
JSJM	37N°20.03'	122W° 5.48'	Z	0.44	
JSLM	37N°34.56'	122W°25.40'	Z	0.23	
JSMM	37N°12.74'	122W°10.06'	Z	0.36	
JSSM	37N°10.17'	121W°55.84'	Z	0.08	
JSTM	37N°12.41'	121W°47.84'	Z	-0.11	751226-801107
JTRM	37N°21.13'	122W°11.88'	Z	0.05	
JWSM	37N°25.08'	122W°16.33'	Z	0.32	700813-720210, 761004-780414
NABM	37N°56.35'	122W°45.53'	Z	0.30	
NBOM	37N°55.28'	122W°43.00'	Z	0.30	
NBRM	38N°15.65'	122W°32.99'	Z	0.41	
NCFM	38N°19.28'	122W°47.73'	Z	0.08	
NFIM	37N°41.90'	123W° 0.00'	Z	-0.03	
NGVM	38N°16.84'	122W°12.89'	Z	0.61	
NHFM	38N° 2.98'	122W°31.34'	E	-0.03	
NHFM	38N° 2.98'	122W°31.34'	Z	-0.03	
NHFM	38N° 2.98'	122W°31.34'	N	-0.03	
NLHM	38N° 7.19'	122W° 8.87'	Z	0.80	
NLNM	38N° 9.15'	122W°42.75'	Z	-0.09	
NMIM	38N° 4.69'	122W°15.44'	Z	0.83	
NOLM	38N° 2.50'	122W°47.64'	Z	-0.12	
NOMM	38N° 2.38'	122W°47.55'	Z	-0.12	
NPRM	37N°59.79'	123W° 0.98'	Z	-0.09	
NSEM	38N°10.96'	122W°27.20'	Z	0.07	
NSPM	38N°12.02'	122W°27.82'	Z	0.07	
NTAM	37N°55.43'	122W°35.70'	Z	0.11	
NTAM	37N°55.43'	122W°35.70'	Z	0.11	
NTAM	37N°55.43'	122W°35.70'	E	0.11	
NTAM	37N°55.43'	122W°35.70'	N	0.11	
NTBM	38N°14.87'	122W°55.86'	Z	-0.22	
NTPM	37N°55.22'	122W°33.78'	Z	0.11	

Table 1, continued. USGS Northern California Seismic Network (NCSN) Stations used to locate earthquakes in this study (C, component; SC, station correction in seconds).

CODE	LATIDUTE	LONGITUDE	C	SC	POLARITY REVERSAL PERIOD*
NVEM	38N°22.36'	122W°26.17'	N	0.43	
NVEM	38N°22.36'	122W°26.17'	Z	0.43	
PCCB	37N°30.00'	122W°22.90'	Z	0.12	

*Previously identified by NCSN.

Table 2. Dates, origin times (GMT), locations, depths and magnitudes of sources used in inversion for station corrections.

USGS Shots

--ORIGIN TIME-				-LAT N--		--LON W--		DEPTH	DUR
YR	MON	DA	HRMN	DEG	MIN	DEG	MIN	KM	MAG
91	MAY	30	930	37	49.67	122	29.41	0.00	2.0
93	MAY	26	808	37	32.41	122	24.35	0.00	1.7
93	MAY	26	802	37	20.14	122	13.94	0.00	1.8
93	MAY	28	704	37	36.46	121	57.91	0.00	1.5
93	MAY	28	800	37	51.89	122	11.29	0.00	1.6
93	MAY	28	906	37	46.79	122	6.96	0.00	1.1
93	MAY	28	908	38	0.23	122	21.87	0.00	1.4

Quarry Blasts

--ORIGIN TIME-				-LAT N--		--LON W--		DEPTH	DUR
YR	MON	DA	HRMN	DEG	MIN	DEG	MIN	KM	MAG
74	NOV	21	2045	37	32.86	122	5.37	0.05	1.8
75	JUL	15	2019	37	32.87	122	5.13	0.23	2.0
75	AUG	20	2209	37	32.84	122	5.01	0.31	1.8
76	JUL	31	0	37	32.84	122	5.28	0.24	1.8
83	JAN	13	14	37	32.68	122	4.73	0.04	1.4
84	JUL	3	55	37	32.90	122	4.92	0.07	1.4
85	FEB	7	2201	37	30.49	122	7.40	0.06	1.8
85	FEB	25	1913	37	30.60	122	7.43	0.06	1.7
85	FEB	28	1907	37	31.00	122	7.27	0.05	1.7
85	MAR	4	1937	37	30.67	122	7.30	0.07	1.7
85	MAR	20	1935	37	30.90	122	7.38	0.05	1.6
85	MAR	25	1938	37	31.20	122	7.48	0.07	1.6
85	OCT	1	2144	37	33.03	122	5.10	0.24	1.2
85	NOV	13	2146	37	33.00	122	5.20	0.12	1.3
89	SEP	5	2347	37	33.20	122	5.31	0.16	1.4
90	OCT	24	2009	37	31.03	122	7.34	0.10	1.3

Table 2, continued. Dates, origin times (GMT), locations, depths and magnitudes of sources used in inversion for station corrections.

Earthquakes

YR	MON	DA	HRMN	LAT N DEG	LAT N MIN	LON W DEG	LON W MIN	DEPTH KM	DUR MAG
72	FEB	12	254	37	47.06	122	12.97	1.90	1.8
72	APR	4	1519	37	47.28	122	15.36	6.60	2.3
72	NOV	14	847	37	39.02	122	11.23	12.16	2.4
73	APR	1	2035	37	25.75	122	14.30	4.34	2.1
73	APR	1	2114	37	25.89	122	14.56	4.57	2.2
73	APR	2	633	37	25.81	122	14.57	4.53	2.1
73	JUN	2	745	37	46.85	122	34.29	8.10	1.9
74	JUN	5	1438	37	46.23	122	28.36	17.98	2.4
78	MAY	5	1437	37	46.49	122	17.10	4.94	2.0
79	DEC	20	1229	37	38.36	122	19.92	2.19	2.5
80	DEC	4	2205	37	49.67	122	18.67	4.21	2.0
84	MAY	24	800	37	30.19	122	12.12	7.55	2.8
84	OCT	29	1611	37	55.85	122	27.71	6.91	2.0
84	NOV	1	1014	37	30.15	122	12.26	8.08	2.3
87	JAN	31	1134	37	36.02	122	18.76	3.54	2.0
88	APR	2	1043	37	36.54	122	22.13	9.54	2.1
88	OCT	25	1111	37	31.76	122	5.86	11.10	2.6
88	OCT	25	1112	37	31.76	122	5.69	11.29	2.8
92	JUN	19	1629	37	37.75	122	22.29	12.58	2.4
93	JUN	27	1145	37	56.60	122	31.95	6.09	2.3
94	JAN	10	1902	37	46.69	122	13.55	3.89	2.6

Once station corrections were calculated specifically for stations within the Bay block proper, we again used VELEST on a subset of the source data to calculate station corrections for 39 additional, more distant stations up to 50 km outside the Bay block (see Figure 5 and Table 1). This expanded coverage provides improved take-off angles for use in determining fault-plane solutions. In this second inversion, all hypocenters and station corrections calculated in the first inversion were held fixed, as was the velocity model. It is notable that the range of the station corrections for the Bay block is -0.22 s to 0.49 s, in contrast to the much larger range of -0.16 s to 1.35 s for the station corrections beyond the Bay block. The larger station corrections occur in the East Bay area and reflect substantially slower velocities in the crust east of the Calaveras fault (Catchings and Kohler, 1993).

In all of the station correction calculations, we used a common correction for stations in close proximity to one another (<3 km apart). In addition, time corrections were applied to the shot travel-times to correct for differences between the velocity model and the true velocities in the vicinity of the crust directly beneath each shot. Each "shot correction" was the station correction for the station closest to the shot.

Once the new station corrections were computed, we relocated the NCSN hypocenters in the study area using our 1-D velocity model for San Francisco

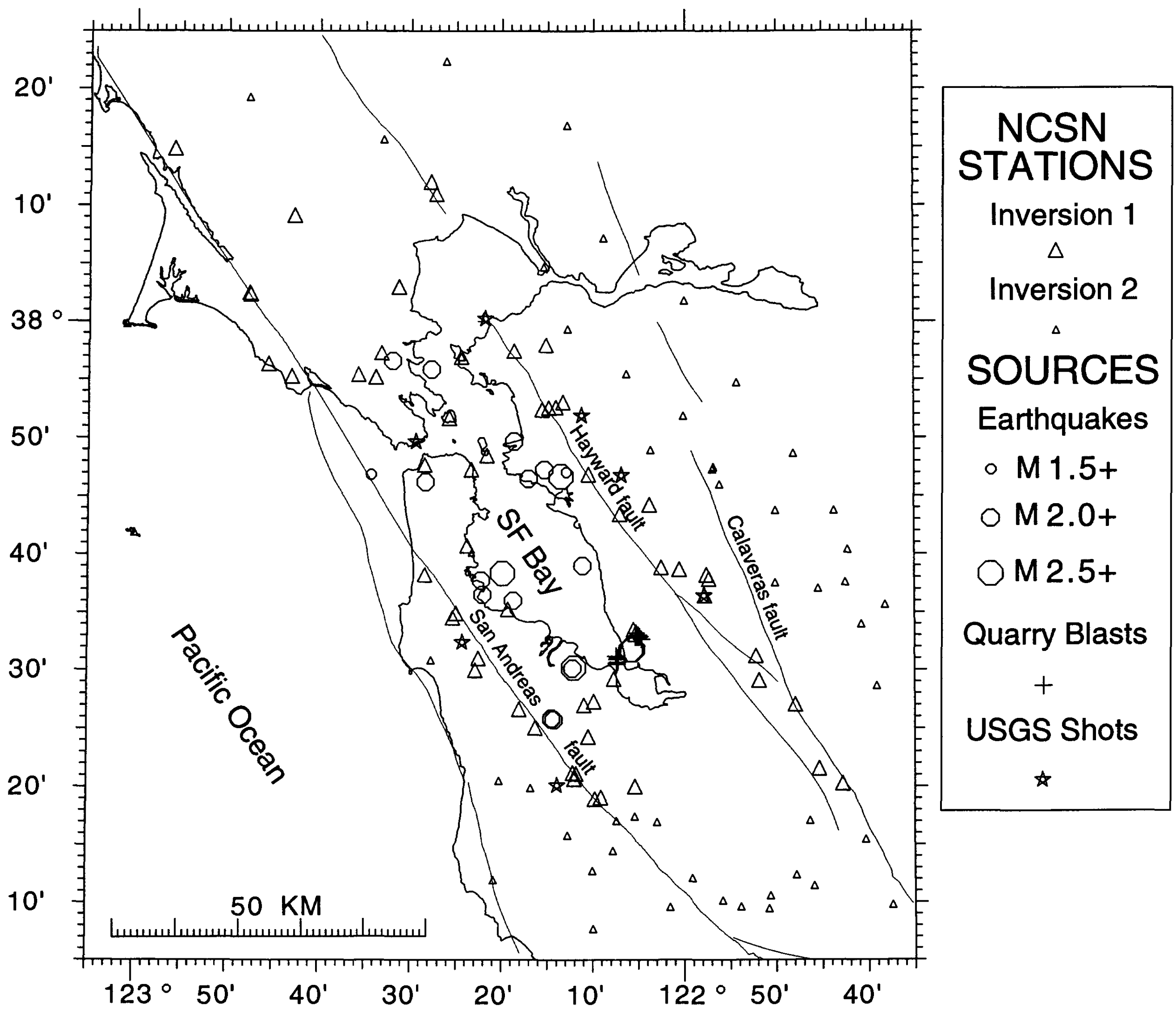

Figure 5. Map showing Northern California Seismic Network (NCSN) station locations and seismic sources (earthquakes, quarry blasts and USGS shots) used in inversion for station corrections and subsequent relocation of Bay block hypocenters. Larger triangles show stations used in inversion for station correction within Bay block (inversion 1), small triangles show stations used in inversion for relative station corrections beyond Bay block (inversion 2).

Bay (Figure 4) in the hypocentral location program HYPOINVERSE (Klein, 1989). We adopted the standard NCSN hypocentral location procedure including calculation of duration (coda) magnitudes (e.g. Oppenheimer et al., 1993).

This relocation procedure resulted in a reduction in the mean root-mean-square (RMS) travel-time residual for the data set, from 0.11 +/-0.08 s for the NCSN locations to 0.09 +/-0.08 s for the new locations, although the actual hypocentral location errors, discussed below (page 18), remain large because of the poor station distribution. This 18% reduction in the mean RMS travel-time residual shows that, while our model provides a small improvement in this parameter, the existing NCSN velocity models appear adequate for locating earthquakes within the Bay block. Further demonstration of a slightly greater precision resulting from the relocation are the improved mean depths of the seven fixed shots which are 1.51 +/-1.78 km and 0.85 +/-0.61 km for the NCSN and new locations, respectively. The epicentral errors for the shots (Figure 6) are, however, about the same for the NCSN and new locations; the mean horizontal errors are 0.71 +/-0.45 km and 0.64 +/-0.41 km, respectively. It should, however, be noted that only one of the shots was located within the Bay block proper, the shot near the Golden Gate. The Golden Gate shot hence provides a more reliable test of our velocity model and station corrections than the other shots. This Golden Gate shot does in fact show that our model is more appropriate for the Bay block proper as the shot is located 0.18 km and 0.61 km from the real location using the new and NCSN model, respectively.

Quarry blast discrimination

Six quarries are located in the study area, and two within 4 km of the study area. All have been active for varying intervals, typically daily to weekly, for all or part of the period of our data set. Other blasts have also occurred in the area intermittently, for example, during construction on the Dumbarton Bridge. Because some of the relocated "earthquakes" in our dataset may have been quarry blasts, and some of the events identified by NCSN as quarry blasts may have been earthquakes, the final step in improving the Bay block seismicity data set involved a careful check to be certain that all events were actual earthquakes, not blasts.

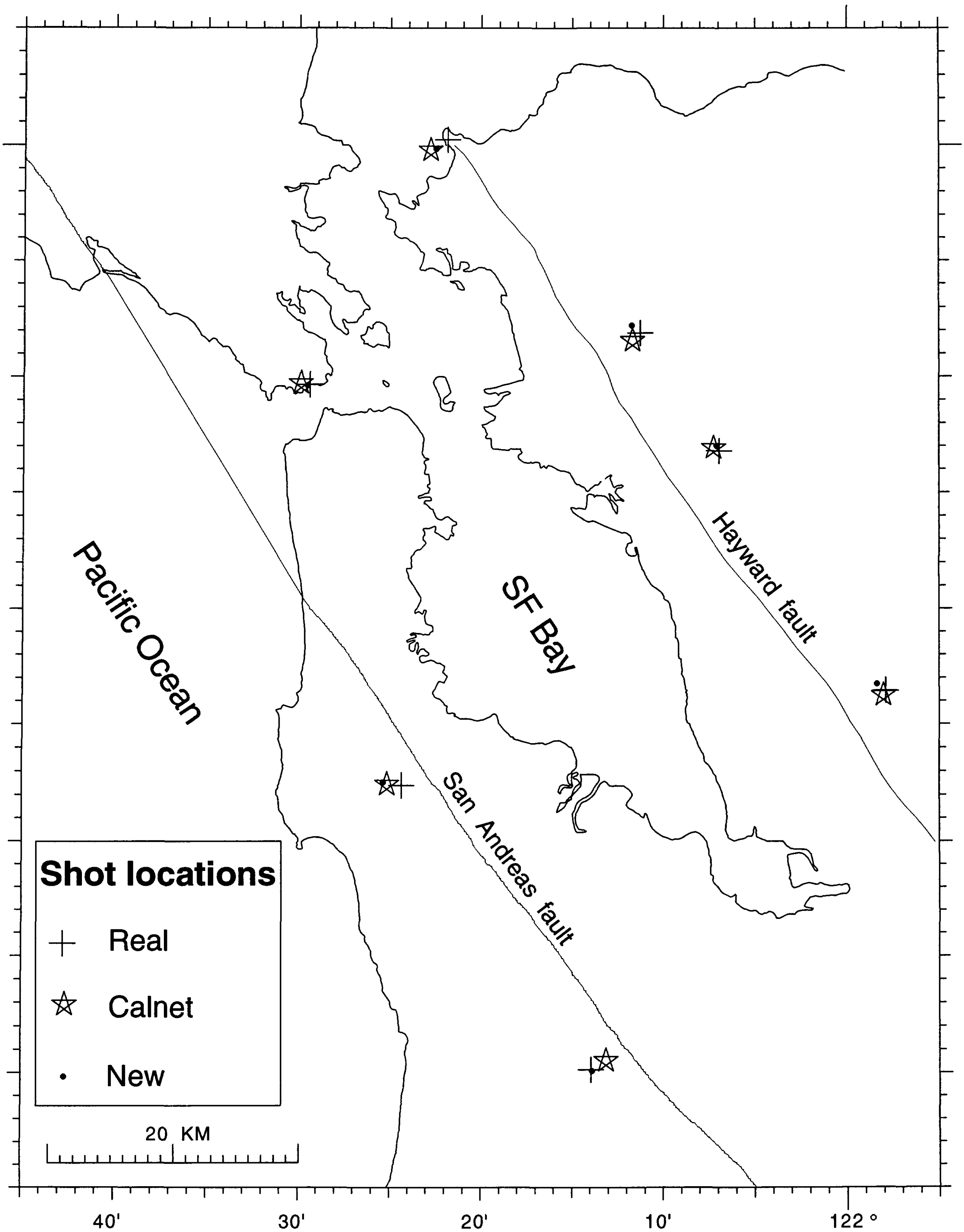

Figure 6. Map showing NCSN, new (this study) and real epicentral locations of shots.

To determine whether any of the events in the vicinity of blast sites were actually unidentified blasts, we followed a set of discrimination criteria similar to that used by NCSN (David Oppenheimer, written communication, 1994): (1) the epicentral location, depth and, in this study, the location errors; (2) the time of day and day of week of the event; and (3) the first-motions at recording stations, because blasts only produce compressional first-motions. We found only two events that NCSN had failed to identify as blasts and omitted them from our earthquake data set. Finally, we also checked the hypocentral parameters of events in the NCSN catalog in our study area identified as quarry blasts, but located more than 10 km from a known quarry site, to determine whether any of these were obviously true earthquakes that were misidentified and archived. We found only one such event (which had eleven clearly dilatational first motions); it was subsequently included in our earthquake data set. All three of these previously misidentified events are now also correctly identified and archived in the NCSN catalog.

Seismicity of the San Francisco Bay Block

Spatial and magnitude distributions

The epicentral locations of 106 well-located M≥1 earthquakes (the present uniform detection threshold) within the San Francisco Bay block (Figure 7) indicate that seismic activity generally falls off with increasing distance from the two major strike-slip faults toward the axis of the bay. Earthquakes are diffusely distributed throughout the Bay block with a concentration of events beneath the San Francisco airport (SFO) and the area east of Oyster Point. In the 26-year period of recording, only 19 well-located earthquakes of M≥2.0, and only two with M=3.0 occurred within the Bay block. The two M3.0 events are located just onshore at the southern end of the Bay, one on the west side near Redwood City and one on the east side near the east end of the Dumbarton Bridge (Figure 7). The persistent cluster of seismic activity beneath SFO includes 22 well-located M≥1.0 events within a source region 2 km in diameter, which is approximately the horizontal location error (see following paragraph). Focal depths for these events range between 8.2-11.5 km, with a mean depth of 10.0 ± 0.8 km.

The well-located events events shown in Figure 7 include 106 (60%) of the 178 M≥1 events located by NCSN in the study area (Appendix A-1). We also identified 51 of the relocated M≥1 events as being poorly located (Appendix A-2), nine as being grossly mislocated or erroneous events (Appendix A-3), and nine as being well-located but processed by machine only, thus possibly not reliable (none of these events are shown in Figure 7). In addition, eleven of the M≥1 events relocated outside the study area, and, as is mentioned above (page 17), two of the NCSN events were blasts, and we identified an additional earthquake that had previously been identified as a blast. The most reliable measure of the true location errors of these events is the location errors for the relocated hypocenter of the single shot within the Bay Block proper, mentioned above (page 15), 0.2 km horizontal error and 0.3 km depth error. However, hypocentral errors vary for each event according to its relative, recording station distribution which is, of course, dependent on the event's magnitude and the operating stations (Klein et al., 1988). Thus, relative location errors for the entire set of events examined in this study can be evaluated using a NCSN standard estimate of the horizontal and depth errors for each event, ERH and ERZ, respectively, calculated by HYPOINVERSE (Klein, 1989). The mean values for ERH and ERZ for the 106 events shown in Figure 7 are 0.4 +/-0.2 km and 1.0 +/-0.4 km, respectively. These error parameters underestimate absolute errors; both ERH and ERZ are about 0.42 times smaller than the principal axes of the 95% confidence ellipsoid for each hypocenter (Klein, 1989).

Figures 8 and 9 are a series of NW-trending cross-sections and depth histograms, respectively, comparing the depth distribution of Bay block seismicity with the seismicity directly adjacent (<3 km) to the bounding San Andreas and Hayward faults. Focal depths of the well-located events within the Bay block are similar to events along both the San Andreas and Hayward faults and are generally less than 15 km, except for three events located 15-16 km beneath San Francisco (km 9-12 in Figure 8), a 15-km-deep event west of San Leandro (km 31 in Figure 8), and an 18-km-deep event along the Hayward fault segment (km 9 in Figure 8). As the histograms demonstrate, most of the background seismicity in all three areas occurs in the depth range of 7-12 km. The relatively shallow (3-7 km deep) seismicity beneath the Hayward fault is spatially associated with the creeping segment of that fault. Similar concentrations of shallow seismicity are observed along the creeping segment of the San Andreas fault in central California (e.g. Hill et al., 1990).

The three events located 15-16 km beneath the city of San Francisco (Appendix A-4) are well located. These events have been re-timed and located with at least 18 P-wave and at least 3 S-wave arrival times. Two of the events, including the largest of these events (M2.4), occurred one day apart (June 4 and 5, 1974) at the same location. The third event occurred 10 years later and is located 10 km to the east beneath the waterfront on the eastern side of San Francisco. The fault-plane solution for the M2.4 event suggests a moderately-dipping (31°W) fault plane as the causative structure.

Temporal distribution

A temporal plot of the well-located M≥1.0 events within the Bay block (Figure 10a) demonstrates that seismicity in the Bay block has occurred persistently throughout the 26-year recording period at an average rate of 4.0 events per year. In addition, the 51 poorly-located M≥1 events listed in Appendix A-2 have also occurred uniformly throughout the period (note that these are not shown in Figure 10a, as many of these also have unreliable magnitudes). Thus, the average rate of occurrence of all the M≥1.0 events in the study area is 5.9 events per year. However, as the largest of these is only M3.0, the total moment release associated with these events within the Bay block in the past 26 years, using a moment/magnitude relation of Bakun (1984), log Mo = 1.2M + 17, is only 4.05 x 10^{21} dyne-cm, approximately equivalent to one M3.8

Figure 7 (opposite). Map showing relocated M≥1 epicenters (circles) in the San Francisco peninsula (Olson and Zoback, 1992) and San Francisco Bay block areas (this study), and NCSN catalog M≥2 epicenters in the East Bay area during the past 26 years (January 1, 1969 through November 25, 1994). Epicenter circles are scaled linearly, proportional to magnitude (1≤M≤5.1). All events located with at least 6 arrival times and have RMS travel-time residual ≤0.3 s, estimated horizontal error (ERH) ≤2 km, estimated vertical error ≤4 km and minimum station distance <20 km. Three adjacent polygons show events in cross-sectional views, depth histograms and temporal plots (Figures 8, 9 and 10, respectively); center polygon is study area. Heavy line in bay shows axis of San Bruno shoal (SBS); dashed lines in bay show axes of aeromagnetic anomaly highs; thin lines in bay show bridges. BK, Berkeley; CP, Coyote Pt.; CS, Crystal Springs Reservoir; DB, Dumbarton Bridge; GG, Golden Gate Bridge; HW, Hayward; MP, Menlo Park; OK, Oakland; OP, Oyster Pt.; PS, Pt. San Pedro; RC, Redwood City; SB, San Bruno Mountain; SF, San Francisco; SFO, San Francisco airport; SL, San Leandro; SMB, San Mateo Bridge; WD, Woodside.

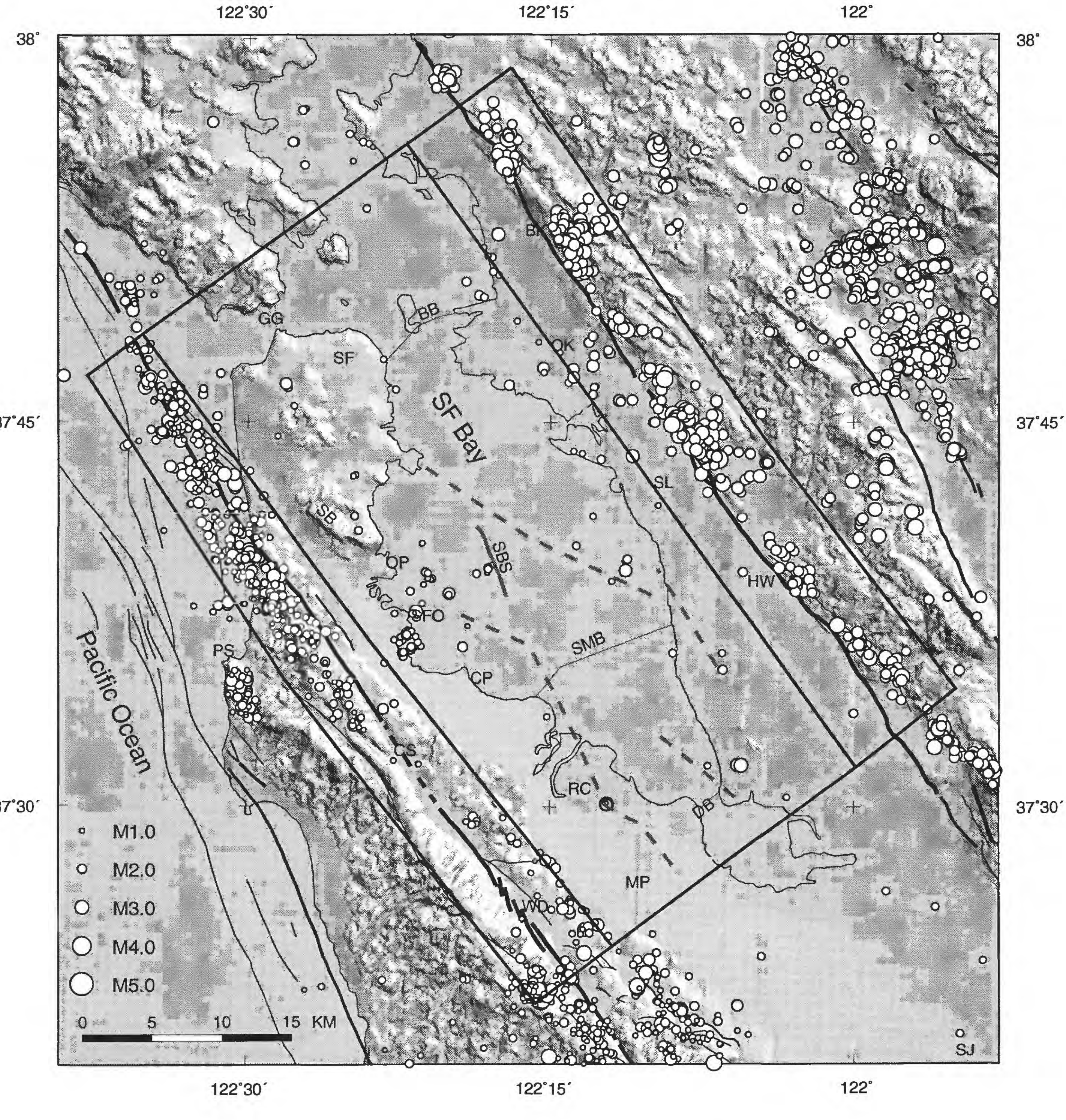

122°30´
122°15´
122°
38°
37°45´
37°30´
BB
GG
SF
SF Bay
OK
SL
SB
OP
SBS
SFO
HW
PS
SMB
CP
Pacific Ocean
CS
RC
DB
MP
WD
SJ
M1.0
M2.0
M3.0
M4.0
M5.0
0 5 10 15 KM

Figure 7.

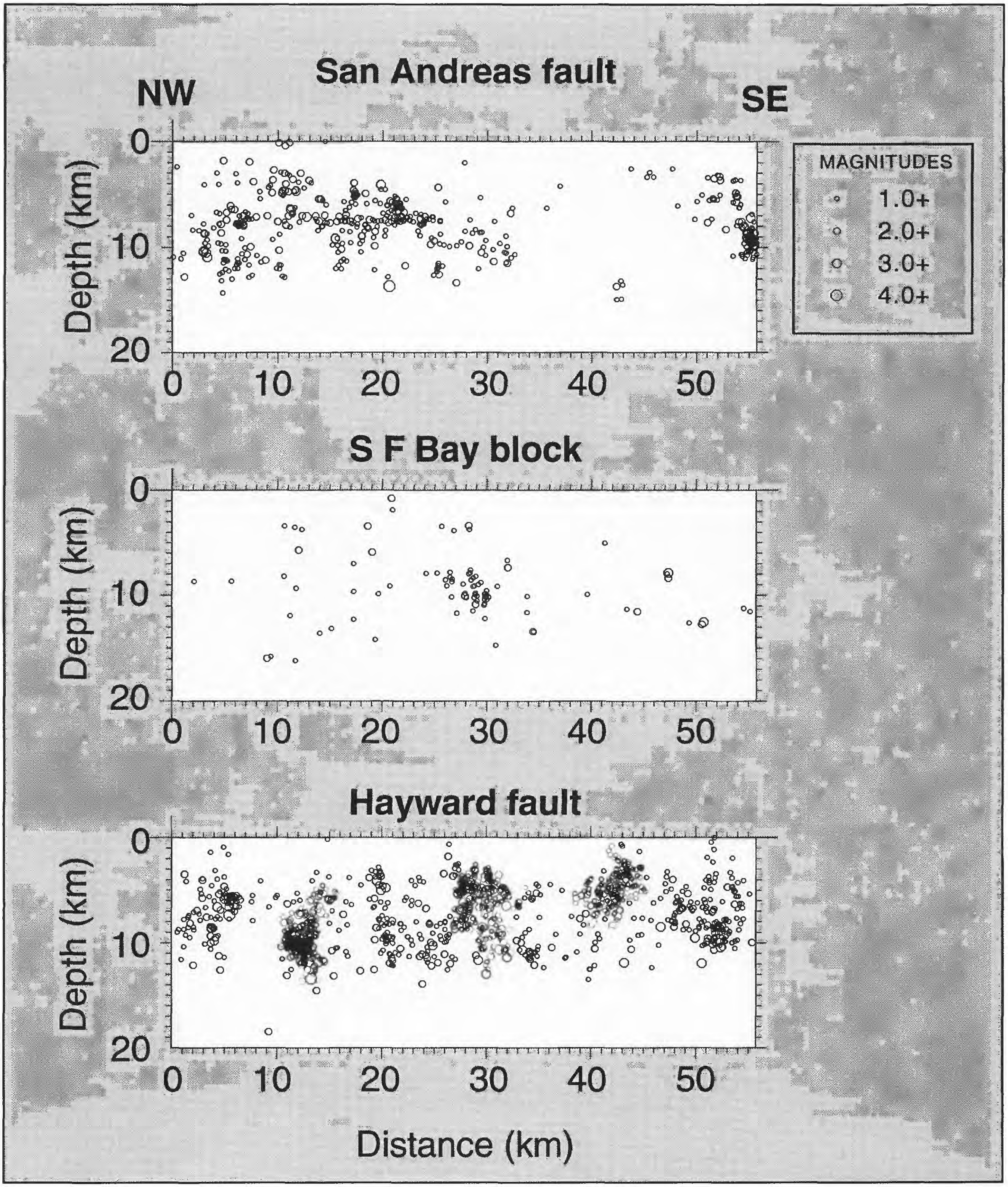

Figure 8. Cross-sectional views of hypocenters of events within three polygons shown in Figure 7. Hypocenters are projected onto a vertical plane beneath NW-SE-trending line in Figure 7 between eastern margin of bay and Hayward fault.

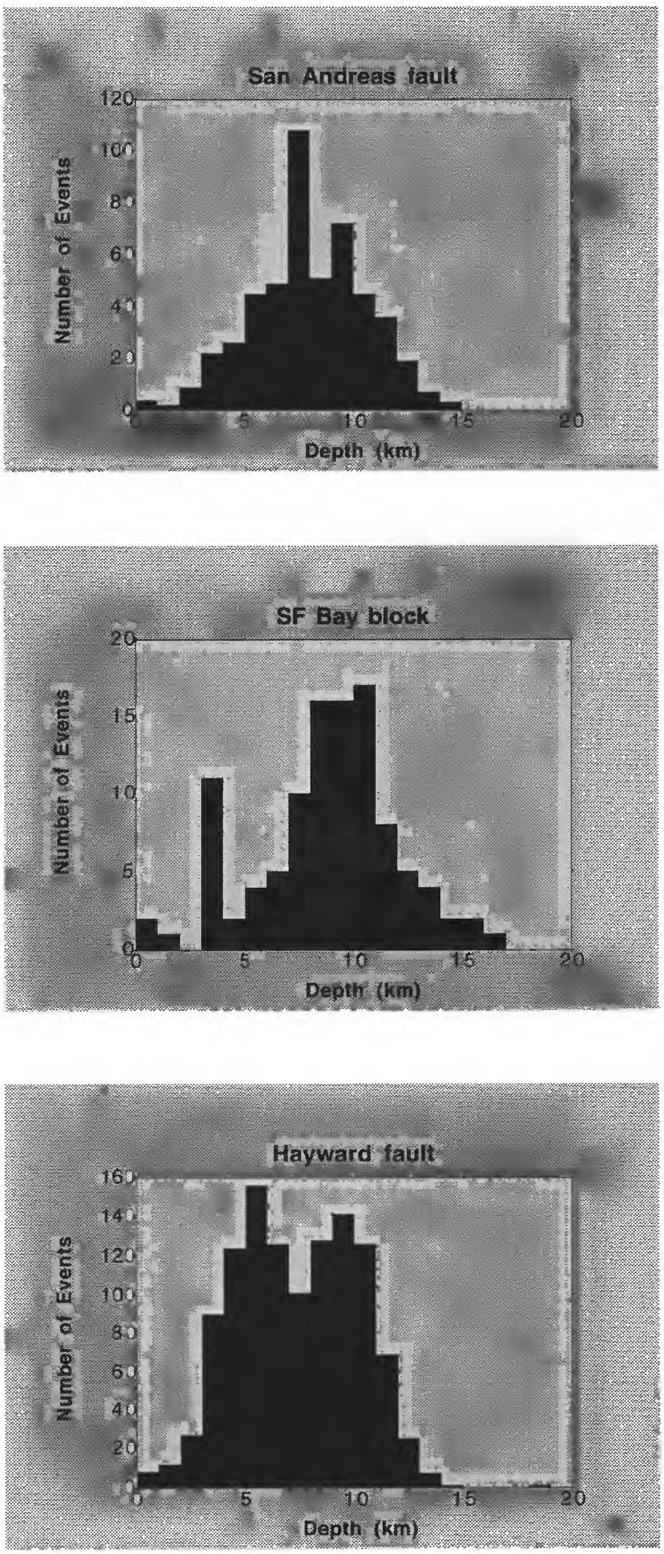

Figure 9. Depth histograms of events within three polygons shown in Figure 7.

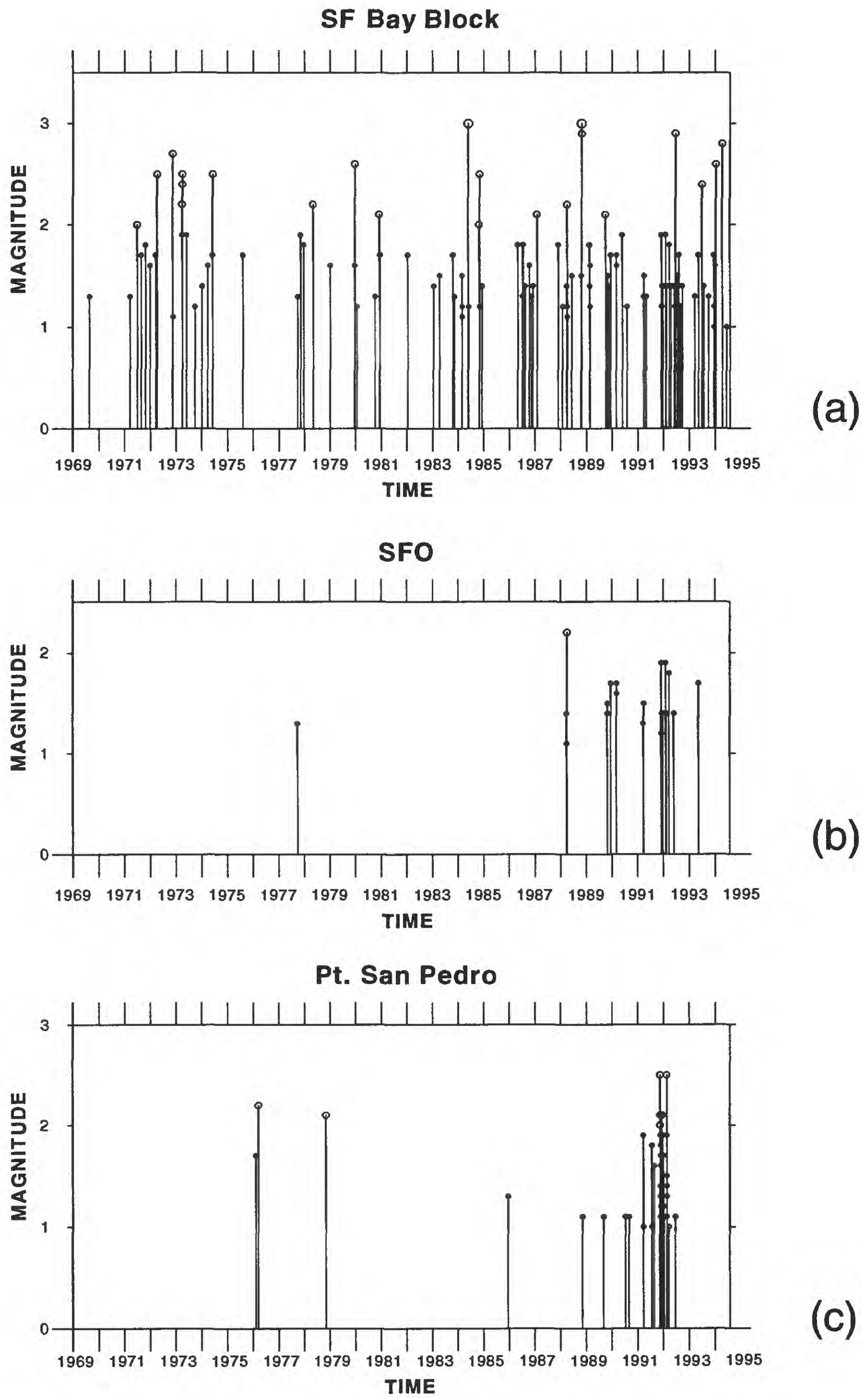

Figure 10. Magnitude vs. time plots for: (a) well-located M≥1 events within San Francisco Bay block (middle polygon in Figure 7), listed in Appendix A-1; (b) M≥1 events in cluster beneath San Francisco airport between 37°N 35'-37' latitude and 122°W 21'-23' longitude, listed in Appendix A-5 (all events in this cluster are well-located), and (c) well-located M≥1 events near Pt. San Pedro between 37°N 33'-36' latitude and 122°W 28'-32' longitude, listed in Appendix A-6.

earthquake. By comparison, the moment release associated with the M1.0-M4.5 events along the adjacent portions of the San Andreas and Hayward faults (within the polygons shown in Figure 7) is 4.35 $x10^{22}$ dyne-cm and 1.07 $x10^{23}$ dyne-cm, respectively, emphasizing that most of the background seismic moment release as well as the major earthquake moment release is dominated by the two through-going, strike-slip fault systems.

Figure 10b, the magnitude and temporal distributions of the 22 well-located M≥1 events beneath the SFO (Appendix A-5), shows that these tightly clustered events began in September 1977 and have continued as recently as May 1993. The largest of these 22 events was a M2.2 event on April 2, 1988. Interestingly, nearly half of the well-located M≥1 events beneath the SFO cluster occurred within a roughly one-year period between March 24, 1991 and March 21, 1992. During this same time period an earthquake swarm occurred 13 km to the WSW beneath the Pacific coast near Point San Pedro (Figures 10c and 11, and Appendix A-6). This Point San Pedro swarm includes 48 well-located M1.0-M2.5 events between March 24, 1991 and March 18, 1992 (33 of these occurred in November and December 1992), located between 4.7-10.3 km depth. This cluster of seismicity beneath Point San Pedro has also been sporadically active; eight events occurred between February 1976 and August 1990 and one occurred in June 1992, in contrast to the 48 events which occurred during the roughly one year time window beginning on March 24, 1991. Similarly, 23 M≥1.0 events occurred during this one year time interval along the San Andreas fault zone between 2 km and 12 km to the north of these SFO and Point San Pedro events, within a persistently active zone which has produced 176 events during the 25.9-year study period (these events are not included in Figure 10). The occurrence of 19% of the events along this portion of the San Andreas fault within this one-year time window represents a seismicity rate about 2.8 times the average rate during the entire study period. This pulse of seismicity between March 1991 and March 1992 appears unrelated to the increase in seismicity following the 1989 M7.1 Loma Prieta earthquake (Reasenberg and Simpson, 1992) (56% of the total events along the northern San Francisco peninsula section of the San Andreas fault occurred in the past 5 years).

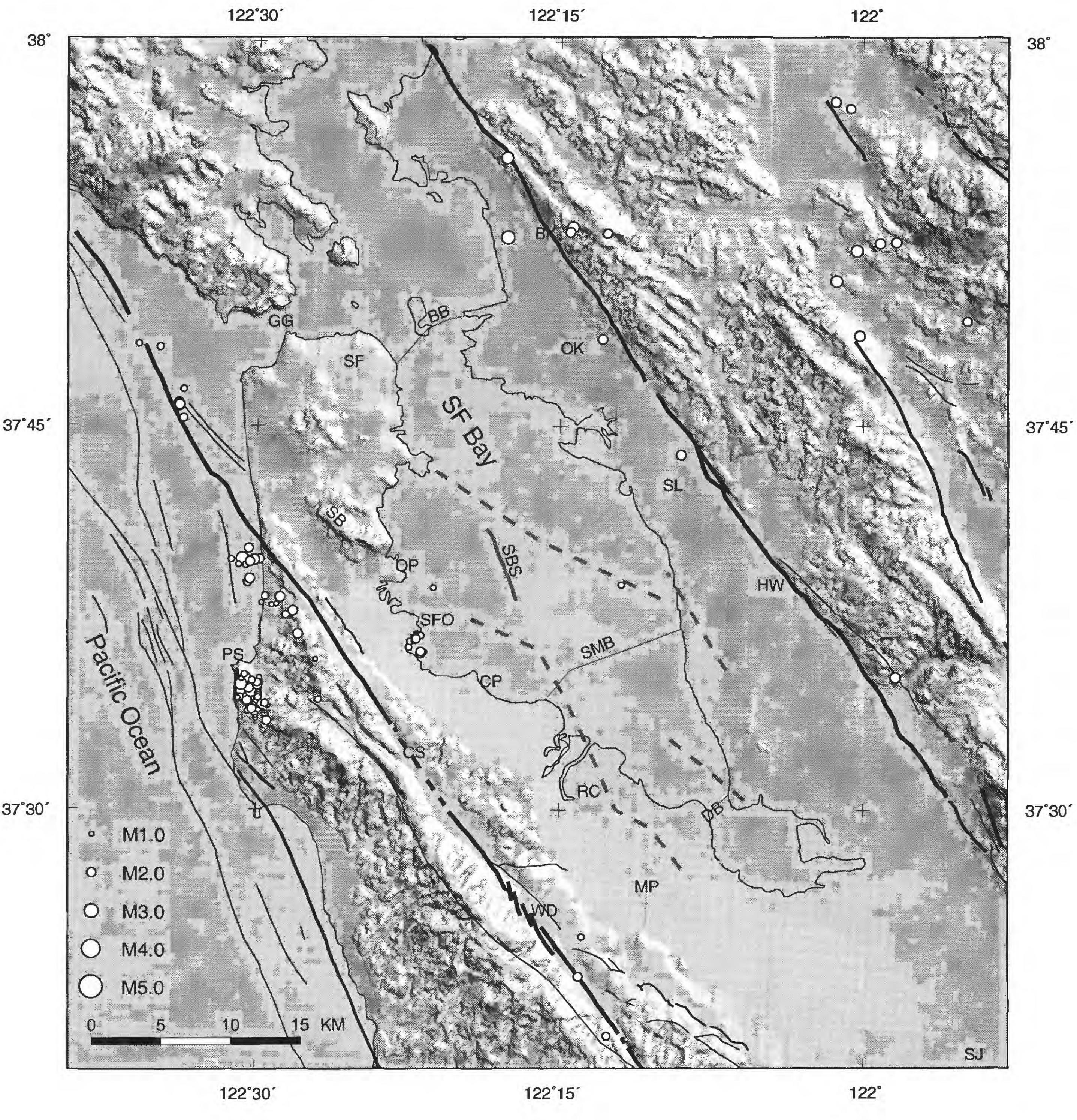

Figure 11. Map showing epicenters of events shown in Figure 7 between March 24, 1991 and March 23, 1992. Heavy line in bay shows axis of San Bruno shoal (SBS); dashed lines in bay show axes of aeromagnetic anomaly highs; thin lines in bay show bridges.

Fault-plane solutions

Fault-plane solutions, shown in Figure 12, were calculated for 14 of the 19 well-located M≥2.0 events within the Bay block (three are composite solutions, two of which include two M≥2 events), each of which had at least ten clear first-motion observations. The fault-plane solutions were calculated with a least-squares, grid-search procedure (FPFIT), which minimizes the number of discrepant first-motions (Reasenberg and Oppenheimer, 1985).

Figure 13 shows the individual first-motion distributions for each of the twelve fault-plane solutions in the Bay block shown in Figure 12, as well as alternate fault-plane solutions for three of the events. Table 3 lists the hypocentral and/or nodal plane parameters for all of the fault-plane solutions. Note that only five of the fault-plane solutions (#6, #9, #10, #11, and #12) are well constrained by the first-motion data, and all of the other fault-plane solutions have one or both nodal planes which are poorly constrained, but the general faulting style indicated by these seven poorly-constrained fault-plane solutions is reliable. Note also that three of the fault-plane solutions are well-constrained composite solutions (see Table 3). Event #6 is a composite of a M3.0 and a M2.5 event which occurred in essentially the same hypocentral area about five months apart, 7.9 km and 8.4 km deep, respectively, with consistent first-motion distributions. Event #9 is a composite of six of the events 9.9 km to 10.8 km beneath SFO with M1.5-2.2; these occurred within a ~five-year period. In this case, the composite was more reliable than the single-event solution for the largest of these events (a M2.2 event in 1988), because the composite includes two events recorded by two critical close-in stations deployed in 1991 at Coyote Point and San Bruno Mountain (JCPM and JSBM, respectively, in Table 1), which better constrain the dip of the NNW-striking nodal plane. The third composite solution, event #10, includes a M2.9 and a M3.0 event, 5.7 km and 5.6 km deep, respectively, which occurred only one minute apart, with consistent first-motion distributions. Events #11 and #12 have fixed depths because the initial depths were too near a layer boundary in the velocity model causing calculated take-off angles to be close to horizontal.

In order to use only the most reliable first-motion observations for the fault-plane solutions in this study, we restricted the values of three parameters as

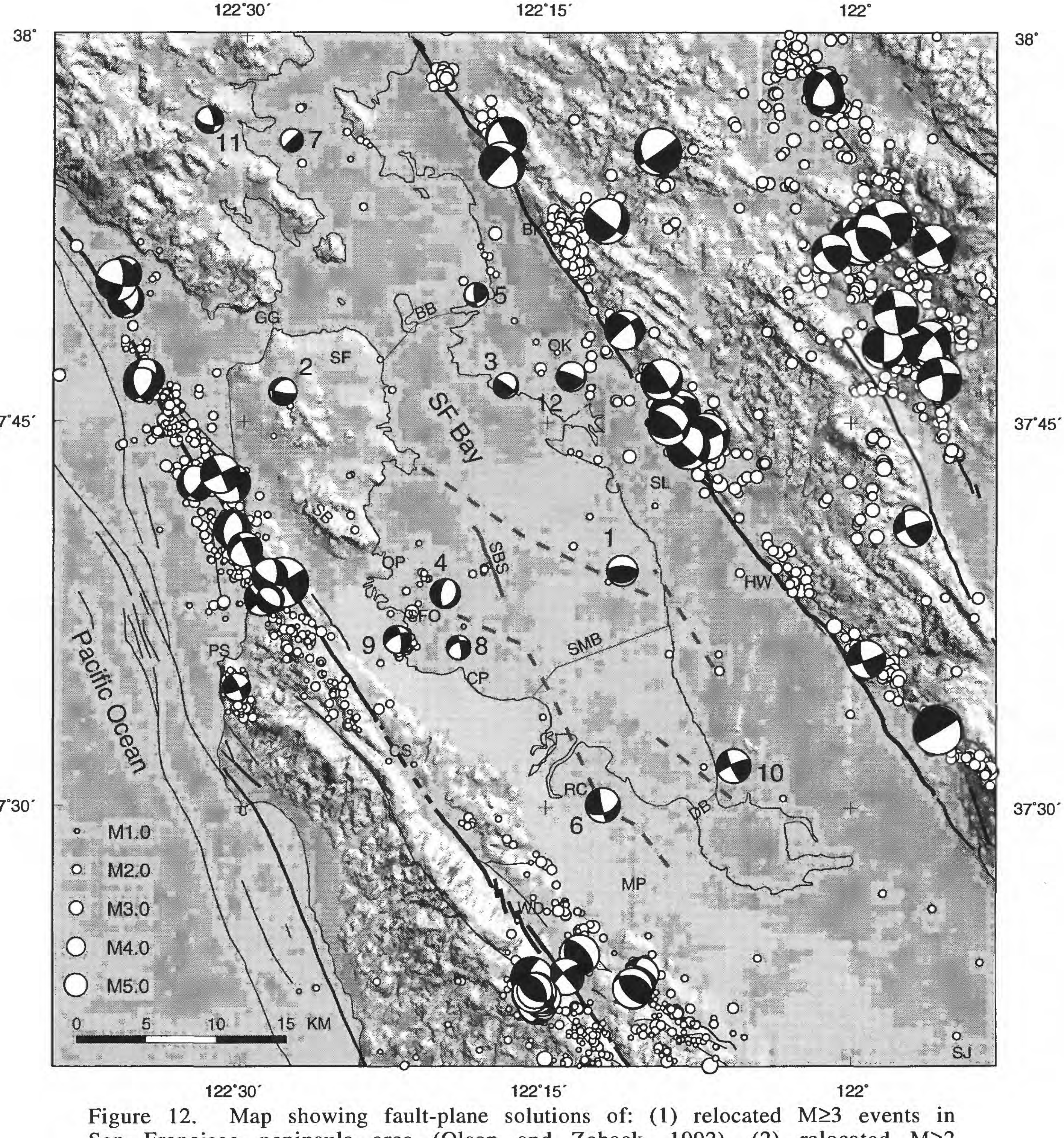

Figure 12. Map showing fault-plane solutions of: (1) relocated M≥3 events in San Francisco peninsula area (Olson and Zoback, 1992), (2) relocated M≥2 events in San Francisco Bay block, and (3) NCSN catalog M≥3.5 events in the East Bay area, as well as some fault-plane solutions of a few smaller events, and some epicenters shown in Figure 7. Circle sizes are scaled linearly, proportional to magnitude (fault-plane solution circles are 2.5 times larger than epicenter circles). Heavy line in bay shows axis of San Bruno shoal (SBS); dashed lines in bay show axes of aeromagnetic anomaly highs; thin lines in bay show bridges. Fault-plane solutions in Bay block are numbered, corresponding to numbers in Figure 13 and Table 3.

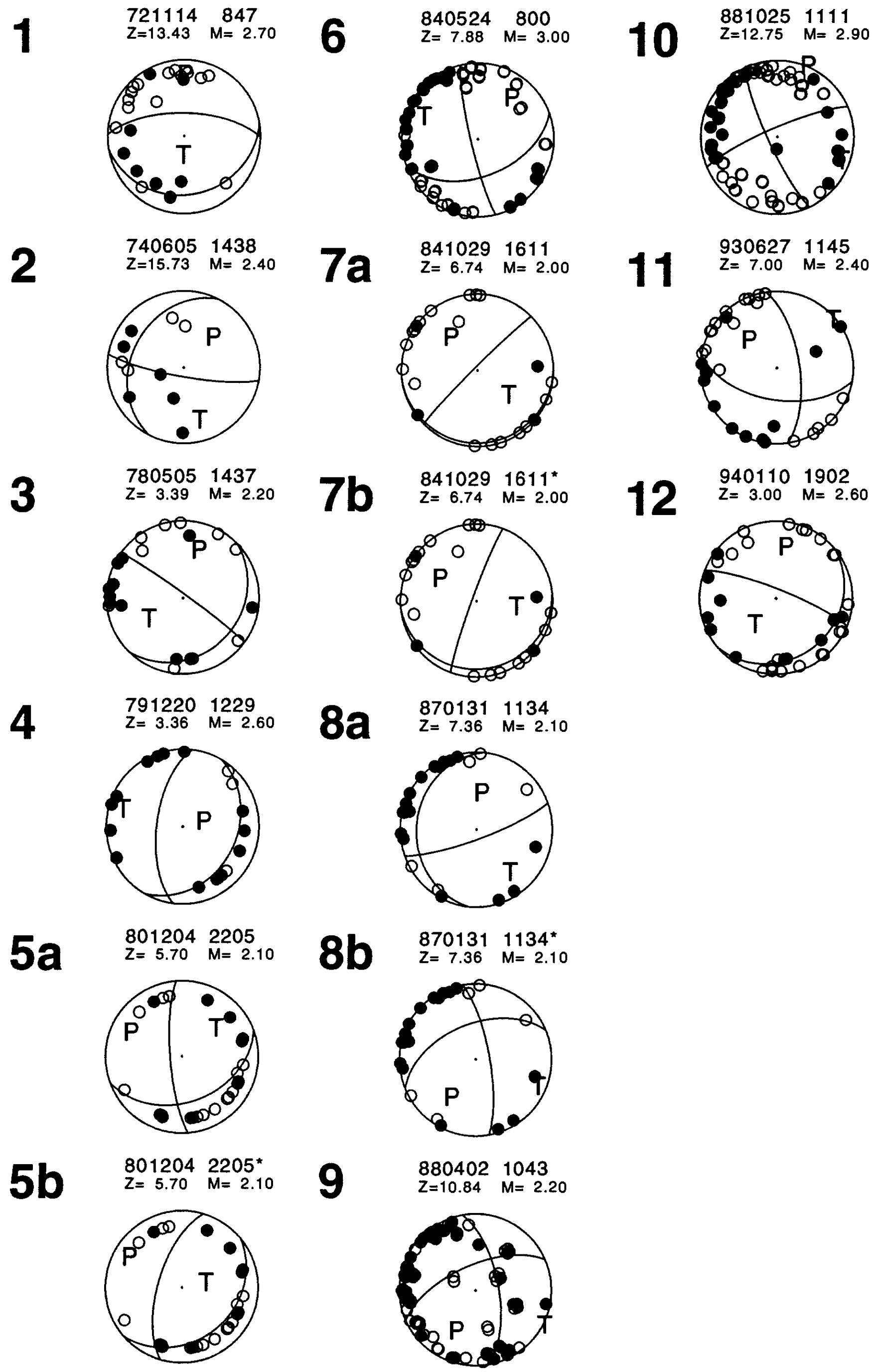

Figure 13. Fault-plane solutions in Bay block shown in Figure 12, with first-motions, and three possible, alternate solutions for events #5, #7 and #8. Solid, open circles, compressional and dilatational first-motions, respectively. P, principal axis of compression; T, principal axis of extension.

Table 3. Fault-plane solution parameters including date; origin time (GMT); location; magnitude; strike, dip rake of each nodal plane; and trend (TRND) and plunge (PLN) of P- and T-axis. Numbers correspond to numbers on map shown in Figure 12 and first-motion plots shown in Figure 13; a,b, alternate fault-plane solutions for same event; C, composite fault-plane solution; *, fixed depth.

NO	ORIGIN TIME				N LATITUDE		W LONGITUDE		DEPTH	DUR	NODAL PLANE 1			NODAL PLANE 2			P-AXIS		T-AXIS	
	YR	MO	DA	HRMN	DEG	MIN	DEG	MIN	KM	MAG	STRK	DIP	RAKE	STRK	DIP	RAKE	TRND	PLN	TRND	PLN
1	72	NOV	14	874	37°	39.23	122°	11.25	13.43	2.7	80°	25°	80°	-90°	65°	95°	-3°	20°	-170°	69°
2	74	JUN	5	1438	37°	46.18	122°	28.09	15.73	2.4	100°	80°	-60°	-153°	31°	-161°	41°	47°	166°	29°
3	78	MAY	5	1437	37°	46.45	122°	17.06	3.39	2.2	45°	25°	10°	-54°	86°	115°	15°	36°	-120°	44°
4	79	DEC	20	1229	37°	38.31	122°	20.02	3.36	2.6	30°	30°	-70°	-173°	62°	-101°	73°	71°	-75°	16°
5a	80	DEC	4	2205	37°	49.99	122°	18.57	5.70	2.1	70°	40°	160°	176°	77°	52°	-66°	23°	48°	44°
5b	80	DEC	4	2205	37°	49.99	122°	18.57	5.70	2.1	50°	30°	120°	-164°	64°	74°	-62°	18°	77°	67°
6C	84	MAY	24	800	37°	30.11	122°	12.17	7.88	3.0	70°	50°	-10°	166°	82°	-140°	36°	33°	-68°	21°
	84	NOV	1	1014	37°	30.09	122°	12.19	8.39	2.5										
7a	84	OCT	29	1611	37°	55.97	122°	27.77	6.74	2.0	85°	5°	130°	-135°	86°	87°	-42°	41°	131°	49°
7b	84	OCT	29	1611	37°	55.97	122°	27.77	6.74	2.0	-160°	85°	80°	84°	11°	153°	-61°	39°	99°	49°
8a	87	JAN	31	1134	37°	36.21	122°	19.34	7.36	2.1	70°	80°	-70°	-174°	22°	-153°	3°	51°	143°	32°
8b	87	JAN	31	1134	37°	36.21	122°	19.34	7.36	2.1	-10°	75°	-140°	-112°	52°	-19°	-144°	38°	114°	15°
9C	88	APR	2	1043	37°	36.51	122°	22.37	10.84	2.2		65°	-150°	-114°	63°	-28°	-151°	38°	118°	1°
	89	OCT	28	1346	37°	36.39	122°	21.57	10.84	1.5										
	90	MAR	5	1855	37°	36.00	122°	22.28	10.37	1.6										
	92	JAN	30	2307	37°	36.19	122°	21.89	9.86	1.9										
	92	MAR	21	1144	37°	36.68	122°	22.11	9.94	1.8										
	93	MAY	11	1559	37°	36.21	122°	21.89	9.87	1.7										
10C	88	OCT	25	1111	37°	31.64	122°	5.73	12.75	2.9	154°	80°	80°	170°	80°	10°	20°	0°	110°	14°
	88	OCT	25	1112	37°	31.63	122°	5.55	12.54	3.0										
11*	93	JUN	27	1145	37°	56.77	122°	31.83	7.00	2.4	100°	55°	55°	-150°	65°	-39°	-48°	44°	48°	7°
12*	94	JAN	10	1902	37°	46.82	122°	13.82	3.00	2.6	50°	20°	20°	30°	80°	108°	7°	33°	-138°	52°

follows: (1) highest precision P-wave arrival-time weights (NCSN weights 0 and 1 out of possible weights 0-4), (2) P-wave travel-time residual (<0.5 s), and (3) the epicentral distance (<70 km). This distance restriction was used because of the large number of observed first-motion discrepancies at epicentral distances beyond 70 km, which apparently result from lateral refraction along the San Andreas and Calaveras faults zones, both of which have documented, large velocity contrasts across them along some sections (e.g. Uhrhammer, 1981; Catchings and Kohler, 1993). In addition, we corrected some first-motions for stations that had electronic polarity reversals. One of the polarity reversals had previously been identified by NCSN (David Oppenheimer, written communication, 1994), and some we detected by tabulating recorded quarry blast first-motions (these should always be compressional). We identified a station as having a reversed polarity if five consecutive, clearly dilatational (0 weight) first-motions were recorded. We lack polarity information for stations and/or periods without clearly recorded first-motion observations for quarry blasts. Table 1 includes the polarity reversal history we used to make these corrections.

Four of the fault-plane solutions shown in Figure 12 show predominantly strike-slip motion. These include the three composite solutions and an event near Oyster Point (#8). All four strike-slip events occur in the southern part of the Bay block and have NNW- and ENE-trending nodal planes. Five of the fault-plane solutions have predominantly dip-slip faulting, three with reverse components (#3, #5 and #12) and two with normal components (#2 and #11). In addition, three of the fault-plane solutions show pure dip slip, one corresponding to reverse/thrust faulting (#1), one to normal faulting (#4) and one to pure vertical or horizontal slip (#7).

Despite the complexity of faulting patterns, the fault-plane solutions indicate a rather consistent variation in deformation style between the northern and southern parts of the Bay block. In the south Bay, **all** five of the solutions have NE-trending P- or B-axes, whereas six of the seven events in the northern part of the block have NNW- to NW-trending P-axes. This along-axes variation is similar to a contrast in deformation style observed in seismicity adjacent to the San Andreas fault on the peninsula (Olson and Zoback, 1992; Zoback and Olson, 1993). Events adjacent to the San Andreas fault from Daly

City north show a maximim horizontal stress (P- or B-axes) subparallel to the San Andreas fault, whereas events south of Woodside (note on Figure 7 that the San Andreas fault between Crystal Springs Reservoir and Woodside is quiescent) indicate primarily thrust-deformation dominated by maximum horizontal compression (P-axes) oriented nearly perpendicular to the San Andreas fault (see Figure 12).

The variation in fault-plane solutions along the San Andreas fault appears related to changes in strike of the fault zone through the peninsula. On the southern peninsula, fault-plane solutions indicate that NE fault-normal compression is most pronounced along a west "bend" in the San Andreas fault, whereas, along the northern peninsula and offshore portion of the San Andreas fault, fault-plane solutions indicate predominantly normal faulting with B-axes subparallel to the San Andreas fault, apparently associated with a ~2-km-wide right step in the fault trace. It is unclear why deformation within the Bay block should show a similar pattern. This variation may represent a broader regional pattern in the stress field with predominant NE-SW directed compression between 37°N-37°N30' latitude and predominant NE-SW- to ENE-WSW-directed extension between roughly 37°N30'-38°N latitude. Such a broad regional pattern and the correlation of deformation style with topography, particularly the correlation of extensional areas with low topographic relief including the track of the Sacramento River, was noted by Simpson et al., (1994), and may reflect broad-scale lithospheric cooling and re-equilibration in response to the passing of the triple junction.

Discussion

Possible active faults within the San Francisco Bay block

Clearly, any deformation of the Bay block is coupled in some way to the regional deformation concentrated along the major, bounding strike-slip faults. Slip along these strike-slip faults could cause internal shear strain within the block and also, possibly, rotation of the block. However, neither the present microseismicity, the high-resolution seismic-reflection profiles within the Bay, nor onshore geologic mapping have provided definitive evidence for active (Holocene) faulting within the block, except for small thrust faults subparallel to the major strike-slip faults (Hart et al., 1981; Page, 1992). The diffuse nature and small magnitudes (M≤3) of the earthquakes within the San Francisco Bay block in the past 26 years, and lack of any obviously aligned fault planes with a consistent sense of slip, suggests that this seismicity is characterized by background volumetric strain release rather than faulting on structures with significant dimensions.

While the microearthquakes within the Bay block demonstrate a potential for brittle failure at depths which commonly correspond to nucleation zones of moderate-to-large earthquakes along the San Andreas fault system, the M≤3 events do not imply the existence of active faults with dimensions sufficient to produce moderate-to-large earthquakes. However, the lack of seismicity defining specific fault structures within the Bay block during this relatively short, 26-year study period does not preclude the existence of such fault zones. If large active faults exist in the Bay block they are presently seismically quiescent. Several recent examples emphasize that moderate-to-large ruptures on buried faults with no surface expression can occur in areas which have been virtually seismically quiescent for at least the preceding decade, including the 1983 Coalinga M6.7 (e.g. Eaton and Rymer, 1990) and the 1989 Loma Prieta M7.1 (e.g. Olson and Hill, 1993) ruptures.

Few of the hypocenters or fault-plane solutions appear to be related to the proposed basement transbay fault zones delineated by prominent aeromagnetic anomalies as suggested by Brabb and Hanna (1981). However, the attitude of such structures at depth is currently undefined. Preliminary modeling by Bob Jachens (written communication, 1994) of the main transbay aeromagnetic high suggests that the source of these linear magnetic highs within the Bay block may be a steep-sided, narrow (3- to 4-km-wide zone of magnetic material in the upper 5 km of the basement. Such a body may represent magnetic material (possibly serpentinites) intruded along an old, subvertical shear zone in the basement. While a small number of epicenters are located within 1 km of an axis of one of the linear aeromagnetic anomalies shown on Figure 7, only three of these were large enough to constrain a fault-plane solution. Only two of these fault-plane solutions (#6, N of Menlo Park and #1, W of Hayward) have a nodal plane consistent in strike to the axis of a linear anomaly. In constrast, the other fault-plane solution (#4, NE of SFO) has nodal planes nearly normal to the axis of the nearby linear aeromagnetic anomaly.

Gravity and seismic-reflection data suggest an additional possible fault-related structure within San Francisco Bay that has probably not been active during the Holocene. As shown in Figure 3, a prominent N30°-35°W-trending elliptical gravity low (maximum anomaly ~ -16mgals) in the east central Bay lies just offshore from San Leandro. Shallow seismic-reflection profiles over this gravity low have revealed a marked unconformity, in which flat-lying, young bay mud sediments truncate steeply east-dipping sediments, possibly part of a buried basin (Marlow et al., 1994). Age of these deformed sediments and the related basin is currently unknown; but the deformation event must be older than 600,000 years based on a maximum thickness of overlying flat-lying bay mud sediments of 300 m (Marlow et al., 1994). Six of the well-located $M \geq 1.0$ hypocenters in the study area occur directly beneath this anomaly area, but as these are 10-15 km deep they are probably unrelated to dipping faults bounding this basin.

Our study also identified three 15- to 16-km-deep events beneath San Francisco. The fault-plane solution of the largest event is poorly constrained but has one moderate-dipping (31°W) nodal plane. These 15 to 16 km-deep events beneath San Francisco may be associated with the distinct, subhorizontal lower crustal layer at about 16-17 km depth inferred from wide-angle reflections observed on a seismic-reflection profile across the Golden Gate channel (Brocher et al., 1994). Near vertical incidence reflection data from the north arm of the Bay (San Pablo Bay) delineate a similar layer at a similar depth with complex internal structure extending into the Moho. Unfortunately, seismic coverage is insufficient to determine if this layer is laterally continuous beneath the Bay, whether it is pervasive throughout the Bay block, or, most importantly, if it even extends across the major strike-slip faults. Page and Brocher (1992) and Furlong et al. (1989) have suggested this regionally extensive lower crustal layer may represent either a thickened slab of oceanic crust or the top of a magmatically underplated layer and may be acting as an active detachment layer, coupling deformation on the San Francisco peninsula and the East Bay.

Seismic and potential aseismic deformation of the San Francisco Bay block

Another potential deformation mechanism within the San Francisco Bay block may be related to secondary or "aseismic" slip incuded by large earthquakes on the San Andreas and Hayward faults. This area is the only place on the San Andreas fault where slip is approximately equally partitioned between two closely-spaced, subparallel, major strike-slip faults. Old faults under San Francisco Bay, such as the postulated faults corresponding to the aeromagnetic anomalies, could possibly slip as secondary structures after large earthquakes on the San Andreas and Hayward faults. Much of the ground deformation associated with the 1989 Loma Prieta earthquake in Northern California and the 1992 Landers and 1994 Northridge earthquakes in Southern California resulted from sympthetic slip on secondary structures not directly connected with the main earthquake rupture itself.

To explore the possibility of such deformation on structures under San Francisco Bay, R.W. Simpson (R.W. Simpson, written communication, 1994; Olson et al., 1994) modeled a basement fault defined by a prominent, NW-trending aeromagnetic anomaly high trend extending across the bay (see Figure 2). The model consisted of a 4-km-deep crack in an elastic half-space that is free to slip in response to applied stress changes. The stress changes applied to one 4-km-long patch near the center of this fault were calculated for historic earthquakes with M≥6.8 that occurred along the adjacent sections of the San Andreas and Hayward fault zones in 1836, 1838, 1868, 1906, and 1989.

Stress changes as large as 5 bars occurred on this particular fault patch. This stress change is comparable to or larger than the stress perturbations experienced by secondary structures in Loma Prieta, Landers, and Northridge earthquakes. In principle, offsets as large as 20 cm are possible if the modeled fault segment is free to slip to a depth of 4 km.

Conclusions

- Earthquakes within the San Francisco Bay block are too few, too small ($M \leq 3.0$) and too diffusely located to delineate potentially hazardous faults within the block. These $M \leq 3$ events correspond to a negligible amount of moment release (approximately equivalent to one M3.8 earthquake), and thus do not provide any evidence for active faults within the block with dimensions sufficient to produce moderate-to-large earthquakes.

- Bay block seismicity shows no clear association with the previously postulated transbay fault zones coinciding with prominent, large-scale linear N30°-60°W-trending aeromagnetic anomalies (Brabb and Hanna, 1981).

- If any extensive active faults exist within the San Francisco Bay block, they are presently seismically quiescent Furthermore, low geodetic shear strain rates (<3 mm/yr) for the Bay block (Lisowski et al., 1991) indicate that any extensive active faults within the block must have long (thousands of years) recurrence intervals.

Acknowledgements

We thank Tom Brocher for a helpful review of the manuscript, and we thank David Hill for providing helpful comments. Robert Simpson kindly assisted us in making the shaded-relief maps. Rick Lester and Bob Somera helped collect seismograms of some events (events beneath San Francisco and some of the USGS shots) and Rick Lester re-timed them. David Oppenheimer provided unpublished computer programs used by NCSN for discriminating quarry blasts (which we modified). Randy Nuss wrote a program for tabulating quarry blast first-motion data. We also acknowledge the NCSN staff for processing and locating earthquakes during the past 26 years.

References Cited

Bakun, W.H., 1984, Seismic moments, local magnitudes, and coda-duration magnitudes for earthquakes in central California, *Bull. Seism. Soc. Am.* **74**, 439-458.

Brabb, E.E. and W.F. Hanna, 1981, Maps showing aeromagnetic anomalies, faults, earthquake epicenters, and igneous rocks in the southern SanFrancisco Bay region, California, *U.S. Geol. Surv. Map GP-932*, scale 1:125,000.

Brocher, T.M., McCarthy, J., Hart, P.E., Holbrook, W.S., Furlong, K.P., McEvilly, T., Hole, J.A., and S.L. Klemperer, 1994, Seismic evidence for a lower-crustal detachment beneath San Francisco Bay, California, *Science* **265**, 1436-1439.

Catchings, R.D. and W. Kohler, 1993, Preliminary results from a 1993 seismic survey of the San Francisco Bay area: East Bay results, *EOS, Amer. Geophys. Union. Trans.* **74**, 413.

Eaton, J.P. and M.J. Rymer, 1990, Regional seismotectonic model for the southern Coast Ranges, *in* The Coalinga, California, Earthquake of May 2, 1983, *U.S. Geol. Surv. Prof. Pap. 1487*, 97-112.

Ellsworth, W.L., 1977, Three-dimensional structure of the crust and mantle beneath the island of Hawii, Ph.D. thesis, Mass. Inst. of Technol., Cambridge.

Furlong, K.P., Hugo. W.D., and G. Zandt, 1989, Geometry and evolution of the San Andreas fault zone in northern California, *J. Geophys. Res.* **94**, 3100-3110.

Hart, E.W., Bryant, W.B., Smith, T.C., Bedrossian, T.L., and D.P. Smith, 1981, Summary report: fault evaluation program, 1979-1980 (Southern San Franicisco Bay Region), *Calif. Div. Mines Geol. Open-File Rept. 81-3 SF*, 12 pp., 1 plate.

Hill, D.P, Eaton, J.P. and L.M Jones, 1990, Seismicity, 1980-86, *in* The San Andreas Fault System, California, *U.S. Geol. Surv. Prof. Pap. 1515*, ed. R.E. Wallace, 115-152.

Hole, J.A., Holbrook, W.S., Klemperer, S.L., Ten Brink, U.S., and T.M. Brocher, 1993, Crustal structure in the San Francisco Bay area from wide-angle refraction data, *EOS, Amer. Geophys. Union. Trans.* **74**, 445.

Jachens, R.C. and C.W. Roberts, 1993, Aeromagnitic map of the San Francisco Bay area, California, *U.S. Geol. Surv. Map GP-1007*, scale 1:286,500.

Klein. F.W., 1989, User's guide to HYPOINVERSE, a program for VAX computers to solve for earthquake locations and magnitudes, *U.S. Geol. Surv. Open-File Rept. 89-314*, 44 pp.

Klein, F.W., Eaton, J.P. and F. Lester, 1988, Seismic station data for northern California and surrounding areas, *U.S. Geol. Surv. Open File Rept. 88-448*, 55 pp.

Kohler, W.M. and R.D. Catchings, 1994, Data report for the 1993 seismic refraction experiment in the San Francisco Bay area, California, *U.S. Geol. Surv. Open-File Rept. 94-241*, 71 p.

Kovach, R.L. and G.C. Beroza, 1993, Seismic potential from reverse faulting on the San Francisco peninsula, *Bull. Seism. Soc. Am.* **83**, 597-602.

Lienkaemper, J.L., Borchardt, G. and M. Lisowski, 1991, Historic creep rate and potential for seismic slip along the Hayward fault, California, *J. Geophys. Res.* **96**, 18261-18283.

Lisowski, M., Savage, J.C. and W.H. Prescott, 1991, The velocity filed along the San Andreas fault in central and southern California, *J. Geophys. Res.* **96**, 8369-8389.

Mann, G.M., Marlow, M.S., and E.E. Brabb, 1993, Newly discovered strike-slip faults in south-central San Francisco Bay, *EOS, Amer. Geophy. Union Trans.* **74**, 693.

Marlow, M.S., Hart, P.E., Childs, J.R., Mann, D.M., Mann, G.M., Carlson, P.R. and R.J. Anima, 1994, A major unconformity beneath south San Francisco Bay and the develpoment of San Leandro Basin, *EOS, Amer. Geophy. Union Trans.* **75**, 683.

Marlow, M.S., Hart, P.E., Carlson, P.R., Childs, J.R., Mann, D.M., Anima, R.J., and R.E. Kayen, 1995, Misinterpretation of lateral acoustic variations as fault offsets as imaged by high-resolution seismic reflection profiling of Holocene muds beneath south San Franicsco Bay, California, submitted to *Marine and Petroleum Geology.*

McCarthy, J. and P. Hart, 1993, Data report for the 1991 Bay Area Seismic Imaging Experiment, *U.S. Geol. Surv. Open-File Rept. 93-301*, 26 pp.

Murphy, J.M., Catchings, R.D., and W.M. Kohler, 1992, Data report for 1991 active-source seismic profiles in the San Francisco Bay area, California, *U.S. Geol. Surv. Open-File Rept. 92-570*, 45 pp.

Olson, J.A. and D.P. Hill, 1993, Seismicity in the southern Santa Cruz Mountains during the 20-year period before the earthquake, *in* The Loma Prieta, California Earthquake of October 17, 1989: Earthquake Occurrence -- Preseismic Observations, *U.S. Geol. Surv. Prof. Pap. 1550-C*, C3-C16.

Olson, J.A. and M.L. Zoback, 1992, Seismic deformation patterns on the San Francisco Peninsula,*EOS, Amer. Geophy. Union Trans.* **73**, 401.

Olson, J.A., Zoback, M.L., Simpson, R.W. and M.S. Marlow, 1994, Deformation of the San Francisco Bay block?, *EOS, Amer. Geophy. Union Trans.* **75**, 683.

Oppenheimer, D. and N. MacGregor-Scott, 1992, The seismotectonics of the eastern San Franicsco Bay region, *in* Proceedings of the Second Conference on Earthquake Hazards in the Eastern San Francisco Bay Area, *Calif. Div. Mines Geol. Spec. Pub. 113*, 11-16.

Oppenheimer, D., Wong, I. and F.W. Klein, 1992, The seismicity of the Hayward fault, California, *in* Proceedings of the Second Conference on Earthquake Hazards in the Eastern San Francisco Bay Area, *Calif. Div. Mines Geol. Spec. Pub. 113*, 91-100.

Oppenheimer, D., Klein, F., Eaton, J. and F. Lester, 1993, The Northern California Seismic Network Bulletin January - December 1992, *U.S. Geol. Surv. Open-File Rept. 93-578*, 45 pp.

Page, B.M., 1982, Modes of Quaternary tectonic movement in the San Francisco Bay region, California, *in* Proceedings of the Conference on Earthquake Hazards in the Eastern San Francisco Bay Area, *Calif. Div. Mines Geol. Spec. Pub. 62,* 1-10.

Page, B.M., 1992, Tectonic setting of the San Francisco Bay region, *in* Proceedings of the Second Conference on Earthquake Hazards in the Eastern San Francisco Bay Area, *Calif. Div. Mines Geol. Spec. Pub. 113*, 1-7.

Page, B.M. and T.M. Brocher, 1992, Thrusting of the central California margin over the edge of the Pacific plate during the transform regime, *Geology* **21**, 635-638.

Reasenberg, P.A. and D.H. Oppenheimer, 1985, FPFIT, FPPLOT, and FPPAGE: FORTRAN computer programs for calculating and displaying earthquake fault plane solutions, *U.S. Geol. Surv. Open-File Rept. 85-739*, 109 pp.

Reasenberg, P.A. and R.W. Simpson, 1992, Response of regional seismicity to the static stress change produced by the Loma Prieta earthquake, *Science* **255**, 1687-1690.

Roberts, C.W. and R.C. Jachens, 1993, Isostatic residual gravity map of the San Francisco Bay area, California, *U.S. Geol. Surv. Map GP-1006*, scale 1:286,500.

Roecker, S.W., Seismicity and tectonics of the Pamir-Hindu Kush region of central Asia, 1981, Ph.D. thesis, Mass. Inst. of Technol., Cambridge.

Simpson, R.W., Lajoie, K.R. and D.H. Oppenheimer, 1994, Inferring blind thrusts in the San Francisco Bay region from earthquake focal mechanisms and averaged topography, *EOS, Amer. Geophy. Union Trans.* **75**, 681.

Urhammer, R.A., 1981, The Pacifica earthquake of 28 April, 1979, *Bull. Seism. Soc. Am.* **71**, 1161-1172.

Zoback, M.L. and J.A. Olson, 1993, Faulting complexity in the 1906 San Francisco earthquake epicentral area, *EOS, Amer. Geophy. Union Trans.* **74**, 411.

Appendix A:
Catalog of Hypocenters

The following catalog of hypocenters within the San Francisco Bay block includes three selected subsets of our relocated hypocenters for the period January 1, 1969 through November 25, 1994 corresponding to well-located events (Appenidix A-1), poorly-located events (Appendix A-2) and grossly mislocated or erroneous events (Appendix A-3). In addition, Appendices A-4 and A-5 include all hypocenters from Appendices A-1 and A-2 for the three 15 km deep events beneath San Francisco and the 24 events beneath SFO, respectively. In addition, Appendix A-6 includes the 57 well-located, M≥1 events beneath Point San Pedro during the same time period. Column headings correspond to calculated origin time (GMT) - year, month, day, hour-minute, seconds; latitude and longitude, depth, duration magnitude, total number of arrival times (P-wave and S-wave) used in location (N RD), number of S-wave arrival times used in location (N S); RMS travel-time residual in seconds; estimated horizontal and vertical error in km (ERH and ERZ, respectively); azimuthal gap in distribution of recording stations (AZ GAP); and minimum epicentral distance to recording station in km (MIN DS).

Appendix A-1. Well-located events within the San Francisco Bay block (within 7-sided polygon with latitude, longitude coordinates: (1) 38°N, 122°W 35'; (2) 38°N, 122°W 26'; (3) 37°N, 32.2', 122°W; (4) 37°N 25.06', 122°W; (5) 37°N 25.06', 122°W 12'; (6) 37°N 36.5', 122°W 24'; (7) 37°N 50', 122°W 35'). Selection parameters include N RD ≥6, RMS ≤0.30 s, ERH ≤2.0 km, ERZ ≤4.0 km and MIN DS ≤20 km. In addition, 11 events were excluded because they had no (or in two cases only one) arrival-times picked by human readers, and sometimes these machine-picked events are not reliable.

--ORIGIN	TIME	(GMT)-			-LAT	N--	--LON	W--	DEPTH	DUR	N	N	RMS	ERH	ERZ	AZ	MIN
YR	MON	DA	HRMN	SEC	DEG	MIN	DEG	MIN	KM	MAG	RD	S	SEC	KM	KM	GAP	DS
69	AUG	19	1118	6.86	37	37.54	122	21.60	10.22	1.3	9		.08	.5	.6	121	8
71	MAR	17	315	38.83	37	33.53	122	15.16	9.90	1.3	8		.03	.4	1.7	91	14
71	JUN	29	1145	25.39	37	35.34	122	6.44	11.53	2.0	21		.09	.3	.8	51	4
71	AUG	23	717	45.77	37	40.78	122	24.52	9.11	1.7	12		.08	.5	1.6	147	12
71	OCT	25	2150	38.06	37	55.07	122	27.25	6.74	1.8	8		.11	.6	1.6	105	7
71	DEC	27	1441	43.86	37	41.35	122	24.73	9.86	1.6	7		.05	1.0	2.3	132	8
72	MAR	18	700	15.40	37	50.92	122	17.86	11.90	1.7	11		.03	.3	1.0	83	12
72	APR	4	1519	54.90	37	47.14	122	15.36	5.90	2.5	17		.09	.3	.6	67	7
72	NOV	14	847	22.66	37	39.23	122	11.25	13.43	2.7	28		.08	.3	.8	64	13
72	NOV	19	1638	23.66	37	39.58	122	11.29	10.11	1.1	12	1	.09	.6	1.6	138	14
74	JAN	7	137	17.31	37	50.78	122	17.59	3.51	1.4	10		.09	.4	1.5	98	13
74	MAR	12	713	30.11	37	38.57	122	21.04	6.86	.7	10		.06	.8	2.9	160	9
74	MAR	29	202	12.64	37	53.39	122	24.18	8.67	1.6	12		.10	.4	1.0	101	4
74	JUN	4	622	44.52	37	46.23	122	27.94	14.76	1.6	24	4	.12	.4	.5	78	7
74	JUN	5	1438	45.86	37	46.18	122	28.09	15.73	2.4	27	3	.09	.3	.4	79	7
75	AUG	8	1022	14.64	37	39.09	122	18.65	7.97	1.7	29		.07	.2	1.3	83	12
77	SEP	25	245	51.73	37	36.48	122	22.73	11.46	1.3	14		.05	.6	1.5	64	4

--ORIGIN TIME (GMT)-					-LAT N--		--LON W--		DEPTH	DUR	N	N	RMS	ERH	ERZ	AZ	MIN
YR	MON	DA	HRMN	SEC	DEG	MIN	DEG	MIN	KM	MAG	RD	S	SEC	KM	KM	GAP	DS
77	NOV	6	1422	39.63	37	50.53	122	19.21	8.22	1.9	38		.09	.2	.9	38	10
77	DEC	22	259	1.47	37	43.57	122	12.49	3.81	1.8	15		.08	.3	1.2	63	7
78	MAY	5	1437	20.02	37	46.45	122	17.06	3.39	2.2	28		.09	.2	.7	47	10
79	JAN	6	859	22.94	37	56.30	122	25.04	6.17	1.6	10		.05	.3	1.6	92	9
79	DEC	19	440	38.19	37	38.89	122	20.87	8.47	1.6	25		.08	.7	2.0	164	10
79	DEC	20	1229	55.84	37	38.31	122	20.02	3.36	2.6	40		.14	.4	.7	141	10
80	JAN	22	252	58.77	37	38.87	122	20.93	8.71	1.2	12		.03	.4	1.6	84	9
80	OCT	4	623	39.98	37	43.88	122	13.85	7.88	1.3	16	2	.06	.2	1.1	66	7
80	DEC	4	2205	53.09	37	49.99	122	18.57	5.70	2.1	44		.12	.2	.4	53	11
80	DEC	16	1941	52.81	37	49.92	122	18.31	3.69	1.7	22		.08	.3	.7	111	11
82	JAN	15	144	29.48	37	55.99	122	24.38	0.03	1.7	12	1	.11	.4	.4	79	14
82	NOV	6	735	2.37	37	36.37	122	21.99	9.34	.9	8		.02	.4	1.0	109	5
83	JAN	17	2214	41.13	37	57.29	122	27.22	10.68	1.4	9	3	.12	.5	1.8	113	11
83	APR	12	120	19.81	37	38.26	122	20.04	3.72	1.5	17	2	.12	.4	1.0	110	12
83	OCT	20	327	11.41	37	38.40	122	21.94	7.83	1.7	26		.13	.4	1.5	79	8
83	NOV	6	1136	33.06	37	42.95	122	24.70	9.63	1.3	12		.05	.3	1.5	114	10
84	FEB	24	59	39.45	37	55.91	122	24.07	8.40	1.5	25	1	.17	.5	1.1	64	8
84	FEB	24	100	21.74	37	55.78	122	23.89	10.77	1.1	12	1	.04	.4	.8	84	8
84	FEB	24	400	51.92	37	55.23	122	24.86	10.45	1.2	24		.21	.5	1.1	71	7
84	MAY	24	800	54.39	37	30.11	122	12.17	7.88	3.0	65	1	.09	.2	.7	40	11
84	MAY	31	1831	55.65	37	42.91	122	24.80	7.00	1.2	11	1	.06	.5	1.5	107	10
84	OCT	29	1611	39.60	37	55.97	122	27.77	6.74	2.0	38		.08	.2	.8	82	8
84	NOV	1	1014	37.92	37	30.09	122	12.19	8.39	2.5	59	1	.07	.1	.6	40	11
84	NOV	1	1037	4.21	37	30.15	122	12.23	7.96	1.2	23		.04	.2	.9	40	11
84	DEC	11	239	59.10	37	47.30	122	23.39	14.78	1.4	25	7	.09	.3	.5	84	7
85	JUL	9	206	3.57	37	38.60	122	21.41	8.25	.9	13		.02	.4	1.3	81	9
86	MAY	1	230	9.47	37	46.91	122	31.35	8.65	1.8	22		.27	.8	2.0	152	4
86	JUL	4	1816	43.27	37	48.98	122	16.66	13.14	1.3	9		.02	.6	1.3	141	10
86	JUL	9	912	52.75	37	39.67	122	11.16	11.61	1.8	42		.06	.2	.8	62	13
86	JUL	17	126	52.89	37	39.14	122	21.18	8.53	1.8	26		.05	.2	.9	108	10
86	AUG	13	1947	39.87	37	30.38	122	3.30	11.20	1.4	16		.06	.4	1.1	75	6
86	OCT	12	445	56.69	37	40.20	122	13.70	14.76	1.6	16		.04	.3	.9	101	16
86	NOV	12	428	46.00	37	51.64	122	34.23	4.76	1.3	9		.02	.8	.5	155	7
86	DEC	2	2144	46.19	37	45.63	122	27.73	3.42	1.4	6		.05	1.4	.9	204	4
87	JAN	31	1134	16.58	37	36.21	122	19.34	7.36	2.1	48		.07	.2	1.4	54	14
87	NOV	28	1343	28.58	37	57.23	122	27.36	8.32	1.8	11		.08	.4	1.2	89	11
88	JAN	29	500	44.20	37	48.17	122	15.59	12.27	1.2	13		.07	.4	1.4	68	8
88	MAR	25	205	49.34	37	36.59	122	22.09	10.06	1.4	8		.04	.6	1.8	134	5
88	APR	1	1922	46.10	37	36.62	122	21.91	8.98	1.1	8		.03	.5	1.3	91	6
88	APR	2	631	3.41	37	38.90	122	21.08	8.30	1.2	34		.08	.3	1.2	63	9

Appendix A, continued
Catalog of Hypocenters

--ORIGIN TIME (GMT)-					-LAT N--		--LON W--		DEPTH	DUR	N	N	RMS	ERH	ERZ	AZ	MIN
YR	MON	DA	HRMN	SEC	DEG	MIN	DEG	MIN	KM	MAG	RD	S	SEC	KM	KM	GAP	DS
88	APR	2	1043	0.40	37	36.51	122	22.37	10.84	2.2	59		.08	.2	.5	47	5
88	JUN	7	1526	23.45	37	39.11	122	21.07	9.10	1.5	10		.05	.4	1.8	106	10
88	OCT	18	438	43.60	37	35.98	122	6.48	11.28	1.5	35		.07	.2	.6	33	6
88	OCT	25	1111	54.84	37	31.64	122	5.73	12.75	2.9	65	3	.08	.1	.5	24	3
88	OCT	25	1112	46.94	37	31.63	122	5.55	12.54	3.0	70	3	.09	.1	.5	24	3
89	FEB	13	625	25.44	37	50.65	122	34.38	3.66	1.8	22	1	.17	.6	.9	154	9
89	FEB	14	1024	12.84	37	50.55	122	34.56	3.14	1.4	9		.16	1.0	1.9	162	9
89	FEB	19	1455	16.57	37	49.99	122	34.65	3.32	1.2	13	2	.16	.9	1.1	195	10
89	FEB	21	1724	46.06	37	46.55	122	14.12	1.85	1.6	13	2	.04	.4	1.4	108	5
89	SEP	28	2046	40.63	37	55.97	122	27.84	5.65	2.1	25		.07	.2	.4	82	12
89	OCT	25	1708	33.47	37	36.23	122	21.41	10.19	1.4	22		.04	.3	1.0	71	11
89	OCT	28	1346	25.51	37	36.39	122	21.57	10.79	1.5	30		.07	.2	.7	59	6
89	NOV	13	2058	45.04	37	26.12	122	9.87	8.94	.8	7		.10	1.6	3.2	166	13
89	NOV	15	522	55.57	37	31.61	122	7.20	12.62	1.4	14		.04	.3	1.2	79	4
89	DEC	12	1029	17.13	37	35.84	122	22.28	10.39	1.7	20		.04	.3	.9	68	4
90	MAR	5	1751	28.68	37	35.98	122	22.36	10.91	1.7	12		.04	.3	1.0	69	4
90	MAR	5	1855	39.28	37	36.00	122	22.28	10.37	1.6	23		.06	.3	.8	70	4
90	JUL	12	837	2.56	37	44.33	122	28.69	7.18		12		.08	1.0	2.1	185	6
90	JUL	29	723	15.87	37	41.78	122	9.66	6.68	1.2	16		.05	.3	1.5	104	10
91	MAR	24	43	4.62	37	36.87	122	22.07	9.17	1.3	9		.03	.5	1.4	96	6
91	MAR	30	314	54.14	37	36.79	122	22.06	9.11	1.5	16		.05	.3	.7	56	6
91	APR	30	1659	3.06	37	38.80	122	11.94	13.44	1.3	14		.08	.5	1.8	106	14
91	NOV	28	1434	6.15	37	38.67	122	21.28	10.16	1.2	10	1	.03	.4	1.1	82	5
91	DEC	3	1137	51.95	37	36.10	122	21.91	9.57	1.9	11	2	.04	.4	1.0	71	5
91	DEC	7	1127	59.27	37	36.18	122	21.73	9.96	1.2	17	1	.05	.3	.7	78	4
91	DEC	11	957	30.94	37	36.36	122	22.48	10.53	1.4	29	1	.08	.3	.6	56	5
91	DEC	23	1332	4.39	37	36.59	122	22.41	10.22	1.4	34		.07	.2	.5	57	5
91	DEC	24	1210	9.75	37	36.15	122	21.96	10.13	1.4	35	1	.08	.2	.5	48	4
92	JAN	30	2307	45.55	37	36.19	122	21.89	9.86	1.9	52	3	.08	.2	.4	59	4
92	FEB	1	1258	25.40	37	36.81	122	21.87	8.21	1.4	40	2	.08	.2	.4	68	5
92	FEB	1	1742	33.41	37	36.35	122	21.88	9.98		7		.02	.8	1.7	137	5
92	FEB	15	1240	29.50	37	36.63	122	22.20	9.79	1.4	44	1	.07	.2	.5	70	5
92	MAR	21	1144	8.03	37	36.68	122	22.11	9.94	1.8	40	1	.08	.2	.5	54	5
92	APR	17	2230	9.49	37	46.96	122	15.33	14.20	1.4	15		.07	.3	1.2	77	7
92	MAY	29	1358	30.74	37	36.60	122	21.67	8.79	1.4	22		.06	.3	.9	48	6
92	JUN	7	746	37.97	37	40.28	122	21.35	7.92	1.2	29		.07	.3	.5	90	4
92	JUN	19	1629	53.26	37	37.59	122	21.66	10.07	2.9	9	1	.04	.5	1.4	92	7
92	JUL	16	731	37.13	37	46.28	122	22.63	13.11	1.5	23	7	.07	.3	.4	72	9
92	AUG	25	628	10.73	37	44.44	122	28.53	9.32	1.2	15		.07	.4	.6	154	6
92	SEP	21	1156	20.13	37	37.51	122	22.71	11.68	1.4	24	1	.07	.3	.6	66	6

Appendix A, continued
Catalog of Hypocenters

--ORIGIN TIME (UT)--					-LAT N--		--LON W--		DEPTH	DUR	N	N	RMS	ERH	ERZ	AZ	MIN
YR	MON	DA	HRMN	SEC	DEG	MIN	DEG	MIN	KM	MAG	RD	S	SEC	KM	KM	GAP	DS
93	MAR	19	1519	33.92	37	43.80	122	13.43	3.43	1.3	24	2	.11	.3	.9	78	7
93	MAY	11	1559	1.56	37	36.21	122	21.89	9.87	1.7	32	1	.07	.2	.5	48	4
93	JUN	27	1145	0.08	37	56.76	122	31.80	6.19	2.4	52	1	.08	.2	.6	65	6
93	JUL	23	741	50.08	37	41.35	122	12.89	12.19	1.4	36	3	.07	.2	.7	87	11
93	SEP	28	623	3.95	37	51.53	122	18.16	4.66	1.3	18	2	.05	.2	.7	59	8
93	DEC	14	841	10.80	37	39.12	122	18.12	8.36	1.0	18	1	.07	.3	1.0	60	7
93	DEC	14	1902	15.01	37	39.42	122	17.89	7.62	1.2	14	2	.06	.3	1.1	82	8
93	DEC	16	206	7.11	37	39.33	122	18.08	7.87	1.7	36	3	.09	.2	.7	32	8
93	DEC	31	530	48.79	37	39.27	122	18.08	8.56	1.6	42	1	.08	.2	.6	46	8
94	JAN	10	1902	37.45	37	46.77	122	13.87	0.76	2.6	60	3	.08	.1	1.0	29	5
94	APR	12	1239	22.35	37	43.70	122	10.93	11.25	2.8	18		.06	.3	1.5	78	18
94	JUN	12	731	47.11	37	37.02	122	19.10	9.13	1.0	28		.05	.2	.6	49	3
94	OCT	14	1645	13.21	37	37.91	122	21.35	8.94	1.3	24	2	.09	.3	.6	79	6
94	OCT	14	1953	7.01	37	37.51	122	21.82	9.81	1.6	13	3	.03	.4	.9	76	7
94	NOV	25	207	34.10	37	35.98	122	8.92	5.06	1.6	24	1	.07	.2	.5	42	7

Appendix A-2. Poorly-located events within the San Francisco Bay block. Selection parameters include N RD ≥4, RMS ≤0.50 s, ERH ≤10.0 km, ERZ ≤20.0 km and MIN DS ≤30 km; well-located events in Appendix A-1 excluded.

--ORIGIN TIME (UT)--					-LAT N--		--LON W--		DEPTH	DUR	N	N	RMS	ERH	ERZ	AZ	MIN
YR	MON	DA	HRMN	SEC	DEG	MIN	DEG	MIN	KM	MAG	RD	S	SEC	KM	KM	GAP	DS
69	JUN	19	2308	23.52	37	58.92	122	27.66	0.08	2.1	13		.31	2.1	15.1	201	21
69	AUG	19	1118	6.86	37	37.54	122	21.60	10.22	1.3	9		.08	.5	.6	121	8
69	DEC	23	104	44.62	37	40.87	122	25.65	1.83	1.5	5		.07	.6	9.2	182	12
70	JAN	27	6	44.05	37	40.75	122	26.41	3.20	1.7	6		.06	1.0	7.3	190	12
70	APR	18	2119	48.29	37	44.67	122	29.44	7.10	1.9	5		.09	2.3	8.1	220	14
70	APR	24	6	34.20	37	55.91	122	25.13	0.07	1.3	6		.08	6.7	9.4	302	8
70	JUL	10	935	54.62	37	33.35	122	13.86	14.66	.9	5		.04	1.1	2.3	193	12
71	MAR	17	315	38.83	37	33.53	122	15.16	9.90	1.3	8		.03	.4	1.7	91	14
71	JUN	29	1145	25.39	37	35.34	122	6.44	11.53	2.0	21		.09	.3	.8	51	4
71	AUG	23	717	45.77	37	40.78	122	24.52	9.11	1.7	12		.08	.5	1.6	147	12
71	OCT	7	1150	29.86	37	40.42	122	22.77	0.71	1.9	10		.12	.6	13.2	172	9
71	OCT	25	2150	38.06	37	55.07	122	27.25	6.74	1.8	8		.11	.6	1.6	105	7
71	OCT	26	44	1.60	37	40.86	122	25.66	0.02	1.7	8		.08	.4	9.3	97	6
71	DEC	27	1441	43.86	37	41.35	122	24.73	9.86	1.6	7		.05	1.0	2.3	132	8
72	FEB	12	254	1.45	37	46.64	122	13.60	0.48	2.1	10		.14	.5	13.9	88	4
72	MAR	18	700	15.40	37	50.92	122	17.86	11.90	1.7	11		.03	.3	1.0	83	12

Appendix A, continued
Catalog of Hypocenters

--ORIGIN TIME (GMT)-					-LAT N--		--LON W--		DEPTH	DUR	N	N	RMS	ERH	ERZ	AZ	MIN
YR	MON	DA	HRMN	SEC	DEG	MIN	DEG	MIN	KM	MAG	RD	S	SEC	KM	KM	GAP	DS
72	APR	4	1519	54.90	37	47.14	122	15.36	5.90	2.5	17		.09	.3	.6	67	7
72	NOV	14	847	22.66	37	39.23	122	11.25	13.43	2.7	28		.08	.3	.8	64	13
72	NOV	19	1638	23.66	37	39.58	122	11.29	10.11	1.1	12	1	.09	.6	1.6	138	14
73	JUN	2	356	42.47	37	45.31	122	30.98	9.60	1.2	8	1	.14	2.3	3.3	219	14
74	JAN	7	137	17.31	37	50.78	122	17.59	3.51	1.4	10		.09	.4	1.5	98	13
74	MAR	12	713	30.11	37	38.57	122	21.04	6.86	.7	10		.06	.8	2.9	160	9
74	MAR	29	202	12.64	37	53.39	122	24.18	8.67	1.6	12		.10	.4	1.0	101	4
74	JUN	4	622	44.39	37	46.33	122	28.02	15.81	1.7	12		.08	.4	.6	123	10
74	JUN	5	1438	45.79	37	46.50	122	28.14	15.98	2.5	21		.08	.3	.5	78	7
75	AUG	8	1022	14.64	37	39.09	122	18.65	7.97	1.7	29		.07	.2	1.3	83	12
77	SEP	25	245	51.73	37	36.48	122	22.73	11.46	1.3	14		.05	.6	1.5	64	4
77	NOV	6	1422	39.63	37	50.53	122	19.21	8.22	1.9	38		.09	.2	.9	38	10
77	DEC	22	259	1.47	37	43.57	122	12.49	3.81	1.8	15		.08	.3	1.2	63	7
78	MAY	5	1437	20.02	37	46.45	122	17.06	3.39	2.2	28		.09	.2	.7	47	10
79	JAN	6	859	22.94	37	56.30	122	25.04	6.17	1.6	10		.05	.3	1.6	92	9
79	JUN	19	1645	2.12	37	43.14	122	23.02	0.05	1.5	9		.04	.4	7.8	95	12
79	JUL	17	1613	20.98	37	43.18	122	22.45	1.12	1.6	9		.05	.6	8.9	141	12
79	SEP	21	1639	28.36	37	43.22	122	22.33	4.99	1.7	4		.02	1.4	8.4	212	12
79	DEC	19	440	38.19	37	38.89	122	20.87	8.47	1.6	25		.08	.7	2.0	164	10
79	DEC	20	1229	55.84	37	38.31	122	20.02	3.36	2.6	40		.14	.4	.7	141	10
80	JAN	22	252	58.77	37	38.87	122	20.93	8.71	1.2	12		.03	.4	1.6	84	9
80	FEB	9	52	44.97	37	59.20	122	27.54	0.04	2.0	22		.17	.5	11.7	135	14
80	MAR	28	1829	6.35	37	43.09	122	22.41	1.79	1.5	5		.02	.8	8.4	143	13
80	APR	2	2207	19.13	37	58.85	122	27.21	0.18	1.9	13		.11	.5	10.6	136	13
80	MAY	7	1643	39.11	37	43.05	122	22.47	4.99	1.7	4		.02	1.3	8.3	174	13
80	JUL	17	1636	40.18	37	43.18	122	22.27	0.03	1.8	14		.07	.3	8.9	88	12
80	OCT	4	623	39.98	37	43.88	122	13.85	7.88	1.3	16	2	.06	.2	1.1	66	7
80	DEC	4	2205	53.09	37	49.99	122	18.57	5.70	2.1	44		.12	.2	.4	53	11
80	DEC	16	1941	52.81	37	49.92	122	18.31	3.69	1.7	22		.08	.3	.7	111	11
81	MAR	8	536	16.14	37	38.80	122	10.48	5.46	1.4	7		.09	1.3	1.4	218	14
81	MAY	12	1907	6.33	37	36.09	122	4.79	0.04	1.0	9		.15	.7	12.9	175	6
81	MAY	22	2314	1.15	37	32.91	122	5.49	0.00	1.2	10		.13	.7	.4	160	0
81	JUN	10	1928	0.34	37	36.74	122	15.57	10.97	1.3	7		.14	.7	2.0	151	16
81	JUN	23	1818	33.39	37	32.95	122	5.11	0.02	1.1	8		.06	1.1	1.2	109	1
82	JAN	15	144	29.48	37	55.99	122	24.38	0.03	1.7	12	1	.11	.4	.4	79	14
82	JUN	10	1844	25.44	37	53.40	122	27.65	19.19	1.5	5		.09	1.6	3.0	122	10
82	JUN	18	1927	8.71	37	43.15	122	21.62	0.16	1.8	29		.09	.2	9.4	42	13
82	AUG	14	2204	25.63	37	31.11	122	6.81	6.82	1.1	4		.01	5.8	6.9	304	19
82	NOV	6	735	2.37	37	36.37	122	21.99	9.34	.9	8		.02	.4	1.0	109	5
83	JAN	10	1630	5.83	37	39.56	122	26.09	6.07	1.5	13	3	.31	1.0	2.9	100	4

Appendix A, continued
Catalog of Hypocenters

--ORIGIN TIME (GMT)-					-LAT N--		--LON W--		DEPTH	DUR	N	N	RMS	ERH	ERZ	AZ	MIN
YR	MON	DA	HRMN	SEC	DEG	MIN	DEG	MIN	KM	MAG	RD	S	SEC	KM	KM	GAP	DS
83	JAN	17	2214	41.13	37	57.29	122	27.22	10.68	1.4	9	3	.12	.5	1.8	113	11
83	JAN	27	1254	52.69	37	34.78	122	21.56	4.87	1.2	4		.00	2.7	1.0	243	5
83	APR	12	120	19.81	37	38.26	122	20.04	3.72	1.5	17	2	.12	.4	1.0	110	12
83	APR	22	1135	12.89	37	44.00	122	26.41	4.24	.5	4		.02	3.6	7.1	170	7
83	OCT	17	1015	11.47	37	43.05	122	24.54	7.89	1.9	28		.09	.2	1.0	57	10
83	OCT	20	327	11.41	37	38.40	122	21.94	7.83	1.7	26		.13	.4	1.5	79	8
83	NOV	6	1136	33.06	37	42.95	122	24.70	9.63	1.3	12		.05	.3	1.5	114	10
84	FEB	24	59	39.45	37	55.91	122	24.07	8.40	1.5	25	1	.17	.5	1.1	64	8
84	FEB	24	100	21.74	37	55.78	122	23.89	10.77	1.1	12	1	.04	.4	.8	84	8
84	FEB	24	400	51.92	37	55.23	122	24.86	10.45	1.2	24		.21	.5	1.1	71	7
84	APR	20	2358	45.21	37	32.43	122	7.22	6.96	.8	4		.06	3.1	6.9	280	14
84	MAY	18	1620	25.93	37	33.44	122	6.69	0.53	1.0	4		.17	4.0	16.0	239	2
84	MAY	24	800	54.39	37	30.11	122	12.17	7.88	3.0	65	1	.09	.2	.7	40	11
84	MAY	31	1831	55.65	37	42.91	122	24.80	7.00	1.2	11	1	.06	.5	1.5	107	10
84	JUN	29	319	50.23	37	31.08	122	12.18	0.02	1.3	6		.26	2.5	20.0	159	12
84	JUL	23	1655	16.63	37	43.08	122	25.83	0.01	1.8	5		.16	1.3	13.5	169	9
84	OCT	29	1611	39.60	37	55.97	122	27.77	6.74	2.0	38		.08	.2	.8	82	8
84	NOV	1	1014	37.92	37	30.09	122	12.19	8.39	2.5	59	1	.07	.1	.6	40	11
84	NOV	1	1037	4.21	37	30.15	122	12.23	7.96	1.2	23		.04	.2	.9	40	11
84	DEC	11	239	58.98	37	47.46	122	23.31	16.19	1.4	11		.05	.5	.9	125	8
84	DEC	11	1731	11.48	37	43.29	122	27.51	18.53	1.8	6		.06	1.4	1.1	162	8
85	JUL	6	1134	11.00	37	49.82	122	21.22	1.38	.8	4		.06	1.4	9.0	236	7
85	JUL	9	206	3.57	37	38.60	122	21.41	8.25	.9	13		.02	.4	1.3	81	9
85	DEC	6	2023	1.11	37	42.79	122	22.97	4.53	1.7	5		.05	1.5	3.5	95	12
86	MAY	1	230	9.47	37	46.91	122	31.35	8.65	1.8	22		.27	.8	2.0	152	4
86	JUL	4	1816	43.27	37	48.98	122	16.66	13.14	1.3	9		.02	.6	1.3	141	10
86	JUL	9	912	52.75	37	39.67	122	11.16	11.61	1.8	42		.06	.2	.8	62	13
86	JUL	17	126	52.89	37	39.14	122	21.18	8.53	1.8	26		.05	.2	.9	108	10
86	AUG	13	1947	39.87	37	30.38	122	3.30	11.20	1.4	16		.06	.4	1.1	75	6
86	SEP	25	1724	18.25	37	27.27	122	5.39	1.98	1.3	7		.16	1.0	14.5	123	13
86	OCT	12	445	56.69	37	40.20	122	13.70	14.76	1.6	16		.04	.3	.9	101	16
86	NOV	12	428	46.00	37	51.64	122	34.23	4.76	1.3	9		.02	.8	.5	155	7
86	NOV	13	646	52.58	37	46.23	122	30.47	0.00	1.8	20	1	.08	.9	.5	240	22
86	NOV	14	2151	18.78	37	32.58	122	5.11	1.58	1.1	6		.07	.4	9.7	103	12
86	DEC	1	315	34.52	37	36.33	122	22.84	10.55	1.3	9		.03	3.3	2.0	286	19
86	DEC	2	722	6.51	37	46.15	122	28.79	5.61	1.8	12	2	.14	3.0	2.9	219	3
86	DEC	2	2144	46.19	37	45.63	122	27.73	3.42	1.4	6		.05	1.4	.9	204	4
87	JAN	5	716	45.43	37	44.66	122	30.05	0.03	1.4	14		.06	1.0	8.1	252	12
87	JAN	31	1134	16.58	37	36.21	122	19.34	7.36	2.1	48		.07	.2	1.4	54	14
87	FEB	10	1736	18.27	37	43.06	122	22.55	4.94	.7	4		.03	1.5	8.4	210	12

Appendix A, continued
Catalog of Hypocenters

--ORIGIN TIME (GMT)-					-LAT N--		--LON W--		DEPTH	DUR	N	N	RMS	ERH	ERZ	AZ	MIN
YR	MON	DA	HRMN	SEC	DEG	MIN	DEG	MIN	KM	MAG	RD	S	SEC	KM	KM	GAP	DS
87	JUN	10	1706	18.48	37	43.14	122	22.48	0.11	1.7	8		.23	.7	18.4	148	12
87	AUG	28	1806	13.88	37	55.61	122	28.11	1.56	2.3	5		.14	2.8	13.7	240	11
87	NOV	4	249	45.32	37	39.38	122	14.35	13.69	1.9	4		.00	1.1	5.0	150	15
87	NOV	7	1845	25.23	37	32.70	122	12.90	6.60	1.3	4		.00	1.0	6.9	154	18
87	NOV	28	1343	28.58	37	57.23	122	27.36	8.32	1.8	11		.08	.4	1.2	89	11
87	DEC	9	1909	57.97	37	41.66	122	27.44	16.96	1.4	6		.01	1.5	.5	237	11
88	JAN	29	500	44.20	37	48.17	122	15.59	12.27	1.2	13		.07	.4	1.4	68	8
88	MAR	25	205	49.34	37	36.59	122	22.09	10.06	1.4	8		.04	.6	1.8	134	5
88	APR	1	1922	46.10	37	36.62	122	21.91	8.98	1.1	8		.03	.5	1.3	91	6
88	APR	2	631	3.41	37	38.90	122	21.08	8.30	1.2	34		.08	.3	1.2	63	9
88	APR	2	1043	0.40	37	36.51	122	22.37	10.84	2.2	59		.08	.2	.5	47	5
88	APR	12	1724	50.61	37	41.66	122	22.11	2.80	1.8	6		.08	.8	3.8	117	11
88	JUN	7	1526	23.45	37	39.11	122	21.07	9.10	1.5	10		.05	.4	1.8	106	10
88	OCT	18	438	43.60	37	35.98	122	6.48	11.28	1.5	35		.07	.2	.6	33	6
88	OCT	25	1111	54.84	37	31.64	122	5.73	12.75	2.9	65	3	.08	.1	.5	24	3
88	OCT	25	1112	46.94	37	31.63	122	5.55	12.54	3.0	70	3	.09	.1	.5	24	3
88	NOV	10	1811	17.41	37	43.51	122	24.33	0.03	1.6	7		.08	.6	9.1	133	10
88	NOV	15	1754	28.25	37	28.12	122	10.61	11.13	2.9	5		.09	.7	.8	150	24
88	NOV	16	1727	47.24	37	40.92	122	23.57	2.41	1.6	7		.29	1.8	6.2	114	9
89	FEB	13	625	25.44	37	50.65	122	34.38	3.66	1.8	22	1	.17	.6	.9	154	9
89	FEB	14	1024	12.84	37	50.55	122	34.56	3.14	1.4	9		.16	1.0	1.9	162	9
89	FEB	16	1614	2.26	37	50.24	122	34.06	1.70	.9	4		.12	1.2	10.8	188	9
89	FEB	19	1455	16.57	37	49.99	122	34.65	3.32	1.2	13	2	.16	.9	1.1	195	10
89	FEB	21	1713	56.28	37	51.55	122	34.24	2.49	1.4	5		.15	1.1	11.0	183	8
89	FEB	21	1724	46.06	37	46.55	122	14.12	1.85	1.6	13	2	.04	.4	1.4	108	5
89	JUN	24	935	53.76	37	25.82	122	7.17	1.79	1.1	4		.01	2.5	6.9	274	6
89	SEP	28	2046	40.63	37	55.97	122	27.84	5.65	2.1	25		.07	.2	.4	82	12
89	OCT	25	1708	33.47	37	36.23	122	21.41	10.19	1.4	22		.04	.3	1.0	71	11
89	OCT	28	1346	25.51	37	36.39	122	21.57	10.79	1.5	30		.07	.2	.7	59	6
89	NOV	13	2058	45.04	37	26.12	122	9.87	8.94	.8	7		.10	1.6	3.2	166	13
89	NOV	15	522	55.57	37	31.61	122	7.20	12.62	1.4	14		.04	.3	1.2	79	4
89	DEC	12	1029	17.13	37	35.84	122	22.28	10.39	1.7	20		.04	.3	.9	68	4
90	MAR	5	1751	28.68	37	35.98	122	22.36	10.91	1.7	12		.04	.3	1.0	69	4
90	MAR	5	1855	39.28	37	36.00	122	22.28	10.37	1.6	23		.06	.3	.8	70	4
90	JUL	12	837	2.56	37	44.33	122	28.69	7.18		12		.08	1.0	2.1	185	6
90	JUL	29	723	15.87	37	41.78	122	9.66	6.68	1.2	16		.05	.3	1.5	104	10
90	AUG	3	1915	55.12	37	58.30	122	27.63	2.13	1.3	5		.03	.7	8.1	133	13
91	MAR	17	235	28.85	37	47.75	122	14.63	1.12	1.5	8		.08	.4	9.0	88	6
91	MAR	24	43	4.62	37	36.87	122	22.07	9.17	1.3	9		.03	.5	1.4	96	6
91	MAR	26	837	8.01	37	47.72	122	14.59	0.62	1.1	10		.08	.4	9.5	65	6

Appendix A, continued
Catalog of Hypocenters

--ORIGIN TIME (GMT)-					-LAT N--		--LON W--		DEPTH	DUR	N	N	RMS	ERH	ERZ	AZ	MIN
YR	MON	DA	HRMN	SEC	DEG	MIN	DEG	MIN	KM	MAG	RD	S	SEC	KM	KM	GAP	DS
91	MAR	30	314	54.14	37	36.79	122	22.06	9.11	1.5	16		.05	.3	.7	56	6
91	APR	30	1659	3.06	37	38.80	122	11.94	13.44	1.3	14		.08	.5	1.8	106	14
91	JUN	3	45	30.68	37	47.59	122	21.91	1.17	.8	4		.09	1.0	10.8	182	9
91	SEP	17	1032	22.30	37	42.60	122	24.30	5.03	1.2	4		.04	2.5	8.1	180	10
91	NOV	28	1434	6.15	37	38.67	122	21.28	10.16	1.2	10	1	.03	.4	1.1	82	5
91	DEC	3	1137	51.95	37	36.10	122	21.91	9.57	1.9	11	2	.04	.4	1.0	71	5
91	DEC	7	1127	59.27	37	36.18	122	21.73	9.96	1.2	17	1	.05	.3	.7	78	4
91	DEC	11	957	30.94	37	36.36	122	22.48	10.53	1.4	29	1	.08	.3	.6	56	5
91	DEC	23	1332	4.39	37	36.59	122	22.41	10.22	1.4	34		.07	.2	.5	57	5
91	DEC	24	1210	9.75	37	36.15	122	21.96	10.13	1.4	35	1	.08	.2	.5	48	4
92	JAN	30	2307	45.55	37	36.19	122	21.89	9.86	1.9	52	3	.08	.2	.4	59	4
92	FEB	1	1258	25.40	37	36.81	122	21.87	8.21	1.4	40	2	.08	.2	.4	68	5
92	FEB	1	1742	33.41	37	36.35	122	21.88	9.98		7		.02	.8	1.7	137	5
92	FEB	15	1240	29.50	37	36.63	122	22.20	9.79	1.4	44	1	.07	.2	.5	70	5
92	MAR	21	1144	8.03	37	36.68	122	22.11	9.94	1.8	40	1	.08	.2	.5	54	5
92	APR	17	2230	9.49	37	46.96	122	15.33	14.20	1.4	15		.07	.3	1.2	77	7
92	MAY	29	1358	30.74	37	36.60	122	21.67	8.79	1.4	22		.06	.3	.9	48	6
92	JUN	7	746	37.97	37	40.28	122	21.35	7.92	1.2	29		.07	.3	.5	90	4
92	JUN	19	1629	53.26	37	37.59	122	21.66	10.07	2.9	9	1	.04	.5	1.4	92	7
92	JUL	16	731	37.09	37	46.27	122	22.69	13.58	1.5	13		.06	.6	1.0	98	9
92	AUG	25	628	10.73	37	44.44	122	28.53	9.32	1.2	15		.07	.4	.6	154	6
92	SEP	21	1156	20.13	37	37.51	122	22.71	11.68	1.4	24	1	.07	.3	.6	66	6
93	MAR	19	1519	33.92	37	43.80	122	13.43	3.43	1.3	24	2	.11	.3	.9	78	7
93	MAY	6	527	43.61	37	46.77	122	15.28	0.95	1.7	9		.04	.4	8.2	93	7
93	MAY	11	1559	1.56	37	36.21	122	21.89	9.87	1.7	32	1	.07	.2	.5	48	4
93	JUN	27	1145	0.08	37	56.76	122	31.80	6.19	2.4	52	1	.08	.2	.6	65	6
93	JUL	23	741	50.08	37	41.35	122	12.89	12.19	1.4	36	3	.07	.2	.7	87	11
93	JUL	24	412	57.83	37	45.90	122	18.53	14.08	1.2	5		.22	5.3	9.4	265	15
93	SEP	28	623	3.95	37	51.53	122	18.16	4.66	1.3	18	2	.05	.2	.7	59	8
93	OCT	13	2100	7.08	37	37.02	122	19.49	7.25	1.3	8		.04	.5	1.1	98	3
93	DEC	14	841	10.80	37	39.12	122	18.12	8.36	1.0	18	1	.07	.3	1.0	60	7
93	DEC	14	1902	15.01	37	39.42	122	17.89	7.62	1.2	14	2	.06	.3	1.1	82	8
93	DEC	16	206	7.11	37	39.33	122	18.08	7.87	1.7	36	3	.09	.2	.7	32	8
93	DEC	31	530	48.79	37	39.27	122	18.08	8.56	1.6	42	1	.08	.2	.6	46	8
94	JAN	10	1902	37.45	37	46.77	122	13.87	0.76	2.6	60	3	.08	.1	1.0	29	5
94	MAR	31	2224	39.82	37	31.77	122	1.19	11.63	.9	4		.04	7.1	3.8	291	21
94	APR	12	1239	22.35	37	43.70	122	10.93	11.25	2.8	18		.06	.3	1.5	78	18
94	MAY	27	1835	31.92	37	59.56	122	26.45	0.01	1.3	4		.06	1.1	8.6	197	6
94	JUN	12	731	47.11	37	37.02	122	19.10	9.13	1.0	28		.05	.2	.6	49	3
94	JUN	20	1718	18.13	37	59.48	122	26.31	1.22	1.2	4		.07	1.0	9.2	198	5

Appendix A, continued
Catalog of Hypocenters

YR	MON	DA	HRMN	SEC	LAT N DEG	LAT N MIN	LON W DEG	LON W MIN	DEPTH KM	DUR MAG	N RD	N S	RMS SEC	ERH KM	ERZ KM	AZ GAP	MIN DS
94	AUG	26	1842	38.18	37	59.47	122	27.20	0.00	1.0	5		.07	.6	4.1	148	6

Appendix A-3. Grossly mislocated or erroneous events within the San Francisco Bay block. These events to not meet the selection criteria for events in Appendix A-2.

YR	MON	DA	HRMN	SEC	LAT N DEG	LAT N MIN	LON W DEG	LON W MIN	DEPTH KM	DUR MAG	N RD	N S	RMS SEC	ERH KM	ERZ KM	AZ GAP	MIN DS
69	APR	2	205	25.40	37	43.53	122	28.00	0.15	2.0	5		.17	11.9	14.3	312	17
78	NOV	8	2343	56.22	37	41.21	122	19.18	0.40	1.8	7		.41	1.6	32.6	126	14
80	APR	26	32	54.93	37	58.98	122	27.01	0.04	2.1	18		.55	1.3	38.3	86	14
83	SEP	20	1845	2.87	37	43.25	122	26.14	0.03	1.3	5		.27	2.5	20.8	151	9
87	NOV	10	1500	52.75	37	44.26	122	16.28	0.65	1.5	4		.29	2.1	21.8	186	19
88	AUG	10	1634	47.58	37	39.70	122	21.21	0.08	1.7	6		.29	1.3	22.5	119	10
88	SEP	21	1637	18.29	37	42.34	122	22.31	0.07	1.6	8		.38	1.2	28.3	90	12
92	DEC	27	1341	59.02	37	32.68	122	19.18	14.74	2.5	7		.04	2.8	.6	290	33
93	OCT	20	1858	34.66	37	26.53	122	2.24	1.32	1.7	4		.16	14.3	13.9	345	13

Appendix A-4. Fifteen-km-deep events beneath San Francisco. These events were re-timed for this study (Rick Lester, written communication 1994) and have very reliable locations.

YR	MON	DA	HRMN	SEC	LAT N DEG	LAT N MIN	LON W DEG	LON W MIN	DEPTH KM	DUR MAG	N RD	N S	RMS SEC	ERH KM	ERZ KM	AZ GAP	MIN DS
74	JUN	4	622	44.52	37	46.23	122	27.94	14.76	1.6	24	4	.12	.4	.5	78	7
74	JUN	5	1438	45.86	37	46.18	122	28.09	15.73	2.4	27	3	.09	.3	.4	79	7
84	DEC	11	239	59.10	37	47.30	122	23.39	14.78	1.4	25	7	.09	.3	.5	84	7

Appendix A-5. Events in a 2 km-diameter cluster beneath SFO (37°N 35'-37' latitude and 122°W 21'-23' longitude. Selection criteria same as for events in Appendices A-1 and A-2, but all events are well-located and meet selection criteria for Appendix A-1.

--ORIGIN	TIME	(UT)--			-LAT N--		--LON W--		DEPTH	DUR	N	N	RMS	ERH	ERZ	AZ	MIN
YR	MON	DA	HRMN	SEC	DEG	MIN	DEG	MIN	KM	MAG	RD	S	SEC	KM	KM	GAP	DS
77	SEP	25	245	51.73	37	36.48	122	22.73	11.46	1.3	14		.05	.6	1.5	64	4
82	NOV	6	735	2.37	37	36.37	122	21.99	9.34	.9	8		.02	.4	1.0	109	5
88	MAR	25	205	49.34	37	36.59	122	22.09	10.06	1.4	8		.04	.6	1.8	134	5
88	APR	1	1922	46.10	37	36.62	122	21.91	8.98	1.1	8		.03	.5	1.3	91	6
88	APR	2	1043	0.40	37	36.51	122	22.37	10.84	2.2	59		.08	.2	.5	47	5
89	OCT	25	1708	33.47	37	36.23	122	21.41	10.19	1.4	22		.04	.3	1.0	71	11
89	OCT	28	1346	25.51	37	36.39	122	21.57	10.79	1.5	30		.07	.2	.7	59	6
89	DEC	12	1029	17.13	37	35.84	122	22.28	10.39	1.7	20		.04	.3	.9	68	4
90	MAR	5	1751	28.68	37	35.98	122	22.36	10.91	1.7	12		.04	.3	1.0	69	4
90	MAR	5	1855	39.28	37	36.00	122	22.28	10.37	1.6	23		.06	.3	.8	70	4
91	MAR	24	43	4.62	37	36.87	122	22.07	9.17	1.3	9		.03	.5	1.4	96	6
91	MAR	30	314	54.14	37	36.79	122	22.06	9.11	1.5	16		.05	.3	.7	56	6
91	DEC	3	1137	51.95	37	36.10	122	21.91	9.57	1.9	11	2	.04	.4	1.0	71	5
91	DEC	7	1127	59.27	37	36.18	122	21.73	9.96	1.2	17	1	.05	.3	.7	78	4
91	DEC	11	957	30.94	37	36.36	122	22.48	10.53	1.4	29	1	.08	.3	.6	56	5
91	DEC	23	1332	4.39	37	36.59	122	22.41	10.22	1.4	34		.07	.2	.5	57	5
91	DEC	24	1210	9.75	37	36.15	122	21.96	10.13	1.4	35	1	.08	.2	.5	48	4
92	JAN	30	2307	45.55	37	36.19	122	21.89	9.86	1.9	52	3	.08	.2	.4	59	4
92	FEB	1	1258	25.40	37	36.81	122	21.87	8.21	1.4	40	2	.08	.2	.4	68	5
92	FEB	1	1742	33.41	37	36.35	122	21.88	9.98		7		.02	.8	1.7	137	5
92	FEB	15	1240	29.50	37	36.63	122	22.20	9.79	1.4	44	1	.07	.2	.5	70	5
92	MAR	21	1144	8.03	37	36.68	122	22.11	9.94	1.8	40	1	.08	.2	.5	54	5
92	MAY	29	1358	30.74	37	36.60	122	21.67	8.79	1.4	22		.06	.3	.9	48	6
93	MAY	11	1559	1.56	37	36.21	122	21.89	9.87	1.7	32	1	.07	.2	.5	48	4

Appendix A-6. Well-located M≥1.0 events beneath the coast near Point San Pedro (37°N 33'-36' latitude and 122°W 28'-32' longitude). Selection criteria same as for events in Appendix A-1.

--ORIGIN	TIME	(UT)--			-LAT N--		--LON W--		DEPTH	DUR	N	N	RMS	ERH	ERZ	AZ	MIN
YR	MON	DA	HRMN	SEC	DEG	MIN	DEG	MIN	KM	MAG	RD	S	SEC	KM	KM	GAP	DS
76	FEB	11	445	59.29	37	33.99	122	29.64	7.67	1.7	21		.07	.5	.4	195	7
76	MAR	17	729	5.19	37	33.83	122	29.82	7.84	2.2	35		.12	.5	.3	182	6

--ORIGIN TIME (GMT)-					-LAT N--		--LON W--		DEPTH	DUR	N	N	RMS	ERH	ERZ	AZ	MIN
YR	MON	DA	HRMN	SEC	DEG	MIN	DEG	MIN	KM	MAG	RD	S	SEC	KM	KM	GAP	DS
78	NOV	8	153	47.09	37	33.44	122	29.92	5.00	2.1	34		.10	.6	1.0	212	6
85	DEC	17	1630	49.25	37	33.68	122	30.32	4.72	1.3	13	3	.05	.6	.3	217	6
88	NOV	7	1102	18.06	37	35.16	122	30.82	10.31	1.1	6		.06	1.8	1.5	241	7
89	SEP	2	2219	26.21	37	33.67	122	30.11	4.46	1.1	22	1	.10	.7	.4	204	6
90	JUL	12	313	33.18	37	33.63	122	30.27	5.10	1.1	16	1	.08	.7	1.5	204	6
90	AUG	30	2217	0.48	37	33.67	122	30.69	4.51	1.1	24		.09	.6	.3	207	7
91	MAR	24	1143	20.96	37	33.46	122	29.48	8.03	1.9	33		.12	.4	.6	201	5
91	MAR	24	1143	30.04	37	33.55	122	30.03	7.07	1.0	7		.04	1.2	.6	219	6
91	MAR	24	1202	37.78	37	33.66	122	30.05	7.39	1.0	10		.05	.9	.5	218	6
91	JUL	25	251	21.26	37	34.10	122	30.30	6.64	1.8	12		.08	1.0	.7	222	7
91	JUL	25	312	31.43	37	34.06	122	29.43	7.46	1.0	13		.07	.9	.5	207	6
91	AUG	26	939	46.64	37	34.15	122	29.57	7.05	1.6	25		.08	.3	.3	126	7
91	NOV	12	1207	37.27	37	34.92	122	29.83	7.26	1.3	14	1	.07	.7	.4	208	6
91	NOV	12	1329	58.54	37	34.71	122	30.38	7.81	1.4	8	1	.02	1.1	.5	215	7
91	NOV	12	1331	9.90	37	34.67	122	30.28	7.43	1.1	11	2	.05	.8	.4	219	7
91	NOV	18	2122	52.52	37	34.69	122	30.27	7.37	1.8	32	1	.10	.5	.3	210	7
91	NOV	18	2124	51.34	37	34.63	122	30.78	7.26	1.9	13		.07	.9	.5	213	7
91	NOV	18	2126	3.03	37	34.75	122	29.94	7.54	1.6	28	2	.09	.5	.3	203	7
91	NOV	18	2128	35.07	37	34.79	122	30.02	7.28	1.9	37	2	.10	.4	.3	196	7
91	NOV	18	2131	35.63	37	34.93	122	30.09	7.58	2.0	35	2	.08	.4	.3	196	7
91	NOV	18	2152	14.32	37	34.26	122	30.45	7.81	1.9	26		.07	.5	.3	205	7
91	NOV	18	2159	14.92	37	34.37	122	30.07	7.40	1.6	17	1	.07	.6	.4	209	7
91	NOV	18	2227	1.50	37	34.39	122	29.97	7.79	1.6	11	2	.05	.8	.5	217	7
91	NOV	19	23	4.60	37	35.16	122	30.53	7.77	1.3	12		.05	.8	.5	211	6
91	NOV	19	207	0.28	37	34.63	122	30.27	7.98	2.5	60	3	.10	.2	.2	127	7
91	NOV	19	207	11.02	37	34.75	122	30.37	7.54	2.0	7	1	.03	.9	1.4	215	7
91	NOV	19	211	59.31	37	34.94	122	30.00	7.68	2.0	49	2	.08	.3	.2	196	6
91	NOV	19	214	1.54	37	35.02	122	30.52	6.81	1.9	40	3	.12	.5	.3	198	7
91	NOV	19	219	29.86	37	34.39	122	30.83	7.83	1.6	17		.06	.7	.3	215	8
91	NOV	19	221	51.67	37	34.88	122	29.95	7.58	2.1	46	2	.10	.3	.2	196	7
91	NOV	19	630	56.37	37	34.53	122	29.91	7.61	1.6	28	2	.08	.5	.3	196	7
91	NOV	19	631	48.51	37	34.44	122	29.92	7.66	1.7	37	2	.09	.4	.3	196	7
91	NOV	19	632	46.02	37	34.35	122	29.90	7.44	1.2	23		.09	.6	.4	208	7
91	NOV	19	1400	45.86	37	33.94	122	30.25	10.05	1.7	12	1	.15	1.7	1.1	212	7
91	NOV	19	1927	33.73	37	33.86	122	30.41	7.15	1.3	17	1	.06	.6	.4	217	7
91	NOV	25	1237	51.91	37	34.20	122	30.03	7.16	1.1	16		.10	.8	.7	204	7
91	NOV	25	1327	43.64	37	34.37	122	29.93	7.55	1.4	31	1	.08	.4	.3	186	7
91	DEC	14	556	5.29	37	35.04	122	29.82	7.87	1.1	13	1	.05	.8	.4	217	6
91	DEC	14	957	27.29	37	33.86	122	30.09	6.33	2.1	8		.04	1.3	.9	228	7
91	DEC	14	1555	16.77	37	34.07	122	30.13	6.92	1.3	30		.09	.5	.3	204	7

Appendix A, continued
Catalog of Hypocenters

--ORIGIN	TIME	(GMT)-			-LAT	N--	--LON	W--	DEPTH	DUR	N	N	RMS	ERH	ERZ	AZ	MIN
YR	MON	DA	HRMN	SEC	DEG	MIN	DEG	MIN	KM	MAG	RD	S	SEC	KM	KM	GAP	DS
91	DEC	15	2348	52.43	37	33.88	122	29.90	7.25	1.1	15	1	.04	.6	.4	214	6
91	DEC	23	207	32.87	37	33.93	122	30.22	7.04	1.9	47		.09	.4	.3	184	7
91	DEC	27	1621	35.99	37	35.16	122	29.87	7.75	1.1	11	1	.06	1.0	.5	222	6
91	DEC	31	1717	9.39	37	34.96	122	30.52	7.61	1.2	24	1	.07	.6	.4	208	7
91	DEC	31	1720	43.94	37	34.96	122	29.96	7.34	1.7	34	2	.09	.5	.3	209	6
92	JAN	5	1808	51.47	37	35.08	122	30.23	8.46	1.2	9	1	.02	.9	1.0	229	6
92	JAN	14	1428	39.13	37	34.36	122	30.92	7.92	1.1	10		.06	1.2	.5	216	8
92	FEB	16	1636	3.24	37	35.26	122	30.47	6.36	1.1	19	1	.07	.5	.6	198	6
92	FEB	16	1646	17.99	37	35.03	122	30.62	7.70	1.3	31	1	.08	.4	.3	188	7
92	FEB	16	1822	41.74	37	35.14	122	30.48	7.41	1.9	44	1	.08	.4	.3	198	6
92	FEB	16	1823	22.55	37	34.90	122	30.76	7.75	2.5	64	1	.10	.3	.3	137	7
92	FEB	16	2106	2.58	37	35.29	122	30.59	7.96	1.4	27	2	.07	.5	.3	198	6
92	FEB	16	2129	37.40	37	35.05	122	30.22	7.06	1.5	21	1	.06	.5	.5	204	6
92	MAR	18	1024	29.50	37	35.11	122	30.73	7.73	1.0	13	2	.04	.8	.5	218	7
92	JUN	20	1158	28.17	37	35.31	122	29.99	7.41	1.1	26	1	.08	.5	.4	196	6